CANCER

Genome-wide CRISPR screen identifies IRF1 and TFAP4 as transcriptional regulators of Galectin-9 in T cell acute lymphoblastic leukemia

Caroline R. M. Wiggers[1,2]†, Burak Yüzügüldü[1,2]†, Nathanial G. Tadros[3], Tayla B. Heavican-Foral[1,2], Eugene Y. Cho[1], Zachary C. Eisenbies[1], Merve Ozdemir[1], Steffen B. Kulp[3], Yun-Cheol Chae[4], Alejandro Gutierrez[4], Jens G. Lohr[2,3,5,6]*‡, Birgit Knoechel[1,2,5,6,7]*‡

Galectin-9 is overexpressed in a variety of cancers and associated with worse clinical outcome in some cancers. However, the regulators driving Galectin-9 expression are unknown. Here, we defined the transcriptional regulators and epigenetic circuitry of Galectin-9 in pediatric T cell acute lymphoblastic leukemia (T-ALL), as an example of a disease with strong Galectin-9 expression, in which higher expression was associated with lower overall survival. By performing a genome-wide CRISPR screen, we identified the transcription factors IRF1 and TFAP4 as key regulators for Galectin-9 expression by binding its regulatory elements. Whereas IRF1 was observed exclusively on the promoter, TFAP4 binding was detected at an enhancer solely in T-ALL cells associated with higher Galectin-9 levels. Together, our results show that IRF1 is responsible and indispensable for Galectin-9 expression and TFAP4 further fine-tunes its expression. Our approach, a flow-based genome-wide CRISPR screen complemented by transcription factor binding and enhancer mapping, creates innovative opportunities for understanding and manipulating epigenetic transcriptional regulation in cancer.

INTRODUCTION

Galectin-9, encoded by the *LGALS9* gene, is a member of the galectin family with carbohydrate-binding domains for β-galactosidases that bind to cell surface and extracellular matrix glycans (*1*–*3*). It has been shown to play a role in a variety of biological processes, including immune responses and tumor progression (*3*, *4*). Although, in some solid tumors, Galectin-9 is associated with an antitumor role by inducing tumor cell apoptosis, it is found to be overexpressed in a variety of cancers and is associated with worse overall survival in some solid and hematologic cancers including pancreatic carcinoma and acute myeloid leukemia (AML) (*4*–*6*). Galectin-9 has been described as an important regulator of the immunosuppressive tumor microenvironment and therefore seen as a promising immunotherapeutic target (*4*, *5*). It is secreted by various immune cell types and binds to multiple receptors including Tim-3, VISTA, and PD-1 (*3*, *5*, *7*–*10*). Binding to Tim-3 on T cells has been described to induce T cell death in CD4+ and CD8+ T cells, whereas PD-1 attenuates this process (*5*). In addition, it has been reported that AML cells secrete Galectin-9 and that its binding to VISTA and Tim-3 induce granzyme B–mediated self-killing in cytotoxic T cells (*10*). In early T cell progenitor acute lymphoblastic leukemia (ETP-ALL), we have previously described a role for Galectin-9 expressed by leukemia cells in mediating CD8+ T cell dysfunction through Tim-3 binding (*11*).

Previous studies have focused on investigating Galectin-9 expression and signaling pathways that induce its expression in hematological cancer cells. It has been shown that Galectin-9 is induced through protein kinase C (PKC) activation by phorbol 12-myristate 13-acetate (PMA) in AML (THP-1) and T cell acute lymphoblastic leukemia (T-ALL) (Jurkat) cell lines (*12*, *13*). In addition, interferon-β/γ (IFN-β/γ) increased Galectin-9 secretion in the AML cell line THP-1 (*5*). However, it is unclear how Galectin-9 levels are regulated on the transcriptional level and the corresponding epigenetic circuitry in hematological malignancies, including T-ALL. T-ALL is a hematologic malignancy originating from developing thymocytes leading to an expansion of malignant T cell lymphoblasts in the peripheral blood and bone marrow (*14*–*16*). Despite achieving overall survival rates up to 80% in children through intensified multiagent chemotherapy, treatment of relapsed/refractory T-ALL remains challenging (*17*–*19*). As Galectin-9 is studied as an immunotherapeutic target in various malignancies, defining its regulation is needed for the development of innovative immunotherapeutic strategies for treatment of T-ALL.

In this study, we defined the transcriptional regulators and epigenetic circuitry of Galectin-9 in pediatric T-ALL, a hematologic malignancy with strong Galectin-9 expression. Similar to what has been observed in some other cancers, high *LGALS9* expression was associated with lower overall survival in pediatric T-ALL. In addition, although all patients did express *LGALS9*, expression was highly variable across patients with T-ALL. We performed a genome-wide CRISPR screen based on intracellular staining of Galectin-9 to identify positive regulators of Galectin-9 in pediatric T-ALL and identified the transcription factors (TFs) IRF1 and TFAP4 to play a role in regulating *LGALS9* expression.

In a pan-cancer analysis, *LGALS9* and *IRF1* were highly expressed in T-ALL and other hematological malignancies compared to a wide range of solid cancer types. Notably, *IRF1* expression showed a strong positive correlation with *LGALS9* across all cancer types and within

[1]Department of Pediatric Oncology, Dana-Farber Cancer Institute, Boston, MA, USA. [2]Harvard Medical School, Boston, MA, USA. [3]Department of Medical Oncology, Dana-Farber Cancer Institute, Boston, MA, USA. [4]Department of Oncology, St. Jude Children's Research Hospital, Memphis, TN, USA. [5]Broad Institute of MIT and Harvard, Cambridge, MA, USA. [6]Huntsman Cancer Institute, University of Utah, Salt Lake City, UT, USA. [7]Department of Hematology/Oncology, Boston Children's Hospital, Boston, MA, USA.
*Corresponding author. Email: birgit.knoechel@hci.utah.edu (B.K.); jens.lohr@hci.utah.edu (J.G.L.)
†These authors contributed equally to this work.
‡These authors contributed equally to this work.

each solid cancer type. However, in pediatric hematologic malignancies such as T-ALL and AML, *TFAP4* showed a strong positive correlation with *LGALS9* expression. Together, our results indicate that *IRF1* plays a key role in regulating *LGALS9* expression in cancer, but in hematologic malignancies that are associated with high *IRF1* expression at baseline, *TFAP4* is responsible for further enhancing *LGALS9* expression.

In T-ALL, we found that IRF1 and TFAP4 regulate *LGALS9* expression by binding its regulatory elements. IRF1 was observed exclusively on the *LGALS9* promoter in multiple T-ALL cell lines with variable Galectin-9 expression. On the other hand, TFAP4 was detected on one enhancer solely in T-ALL cell lines associated with strong Galectin-9 expression and was required for fine-tuning *LGALS9* expression. Together, our results show that promoter-bound IRF1 is responsible and indispensable for *LGALS9* expression and enhancer-bound TFAP4 is responsible for further enhancing *LGALS9* expression in T-ALL. Our approach, a flow-based genome-wide screen complemented by various validation techniques, creates innovative opportunities for understanding and manipulating epigenetic transcriptional regulation in cancer.

RESULTS

LGALS9 expression associated with adverse clinical outcome in T-ALL

To investigate *LGALS9* expression in hematological malignancies compared to solid cancers, we examined its expression at initial diagnosis across primary cancer patient samples in The Cancer Genome Atlas (TCGA; $n = 11{,}607$) and the Therapeutically Applicable Research to Generate Effective Treatments (TARGET; $n = 3118$) pediatric cancer initiative database using the UCSC Xena platform (*20*). Acute lymphoblastic leukemia (ALL) patient samples showed highest expression of *LGALS9* in primary cancer samples at diagnosis (Fig. 1A). This was similarly reflected in cancer cell lines, where hematologic malignancies, including T-ALL, displayed highest expression compared to a wide range of solid cancer cell lines (Fig. 1B) [Cancer Cell Line Encyclopedia (CCLE) 24Q2, $n = 1437$ (*21*)].

In pediatric T-ALL, *LGALS9* expression was heterogeneous across T-ALL subtypes based on oncogenic subtype (TARGET T-ALL initiative, $n = 265$), demonstrating expression levels similar to normal thymocytes but higher than normal peripheral blood T cells (Fig. 1C). TLX1 and TLX3 subtypes were significantly enriched in patients expressing low *LGALS9* in two independent cohorts [TARGET T-ALL initiative and Gabriella Miller Kids First Pediatric Research Program (COG AALL0434)] (Fig. 1D). On the other hand, LMO2 subtypes were associated with high *LGALS9* expression in both cohorts (Fig. 1D). Similarly, T-ALL cell lines also displayed variable *LGALS9* expression across T-ALL subtypes (Fig. 1E). To test whether this was reflected on the protein level, we selected six T-ALL cell lines and quantified Galectin-9 protein by Western blot. We detected highest Galectin-9 protein expression in Jurkat and CCRF-CEM T-ALL cell lines and lowest in HPB-ALL (Fig. 1F). Moreover, these differences were also reflected in secreted Galectin-9 levels in supernatant after 2 days of culture (Fig. 1G).

As we observed heterogeneous *LGALS9* expression in pediatric T-ALL, we sought to investigate the clinical relevance of Galectin-9 in pediatric T-ALL. Notably, we observed higher *LGALS9* expression at initial diagnosis in pediatric patients with T-ALL with poor outcome compared to those who survived [enrolled on COG AALL0434 (Gabriella Miller Kids First Pediatric Research Program ($n = 933$)] (Fig. 1H). Thus, *LGALS9* expression is clinically relevant in pediatric T-ALL and displays heterogeneous expression in cell lines and across patients with T-ALL.

Genome-wide CRISPR screen for Galectin-9 regulators in T-ALL

To identify key players in the regulation of Galectin-9 in T-ALL, we designed a genome-wide CRISPR screen based on fluorescence-activated cell sorting (FACS). To ensure FACS-based Galectin-9 readout is reliable, we analyzed Galectin-9 intracellular expression in T-ALL cell lines expressing high (Jurkat and CCRF-CEM), mid (Loucy), or low (HPB-ALL) Galectin-9 according to total Galectin-9 protein levels as quantified by Western blot (Fig. 1F). For all cell lines, we included Galectin-9 single-cell–derived knockout (KO) clones and scrambled control cell lines (fig. S1A). All cells stained positive for Galectin-9 by intracellular flow cytometry analysis at variable levels similar to our Western blot results (Fig. 2A). Moreover, single-cell–derived Galectin-9 KO cell lines displayed significantly lower Galectin-9 intensity compared to scrambled controls in high Galectin-9 expressing cell lines Jurkat and CCRF-CEM (Fig. 2A). Therefore, we designed a genome-wide CRISPR screen using a FACS readout of intracellular Galectin-9.

We performed two independent genome-wide screen replicates in Jurkat cells, a pediatric T-ALL cell line belonging to the TAL-1 subtype that displayed high Galectin-9 expression (Figs. 1F and 2A). We used the human CRISPR KO pooled Brunello lentiviral CRISPR library targeting 19,114 protein-coding human genes with four single-guide RNAs (sgRNAs) per gene and 1000 control sgRNAs (*22*). As T-ALL cell lines silence Cas9 over time, we freshly generated lentiviral Cas9-expressing Jurkat cells and validated Cas9 activity using the pXPR green fluorescent protein (GFP) plasmid before each screen (see Materials and Methods). Subsequently, Jurkat cells were transduced with the Brunello library at a multiplicity of infection (MOI) of 0.25 with ~650-fold coverage per sgRNA. On day 7, we stained cells for intracellular Galectin-9 and sorted for 20% low and 20% high Galectin-9 expressing cells (fig. S1B), followed by de-cross-linking, genomic DNA (gDNA) isolation, sgRNA amplification, and next-generation sequencing (Fig. 2B). We applied the model-based analysis of genome-wide CRISPR-Cas9 knockout (MAGeCK) algorithm to assess enriched sgRNA abundance in the Galectin-9 low compared to Galectin-9 high populations (*23*). sgRNAs with a positive fold change indicate a positive regulator of Galectin-9, as its KO decreases Galectin-9 expression. Reassuringly, we detected *LGALS9* as top hit in both replicates with a false discovery rate (FDR) of <0.1 (Fig. 2C). Other hits included several TFs, of which *IRF1* was the top scoring hit that showed a highly significant enrichment in the Galectin-9 low population (Fig. 2C).

Validation CRISPR screen identifies IRF1, TFAP4, and ADD1 as hits

To eliminate false-positive hits in the genome-wide screen, we performed a validation screen in Jurkat T-ALL cells in duplicates. We designed a minipool including significant hits (41 enriched and 38 depleted sgRNAs in Galectin-9 20% low gate versus 20% high gate) and 100 control guides. Similar to the genome-wide screen as described before, lentiviral Cas9-expressing Jurkat cells were infected with the lentiviral validation pool and sorted for 20% low and 20%

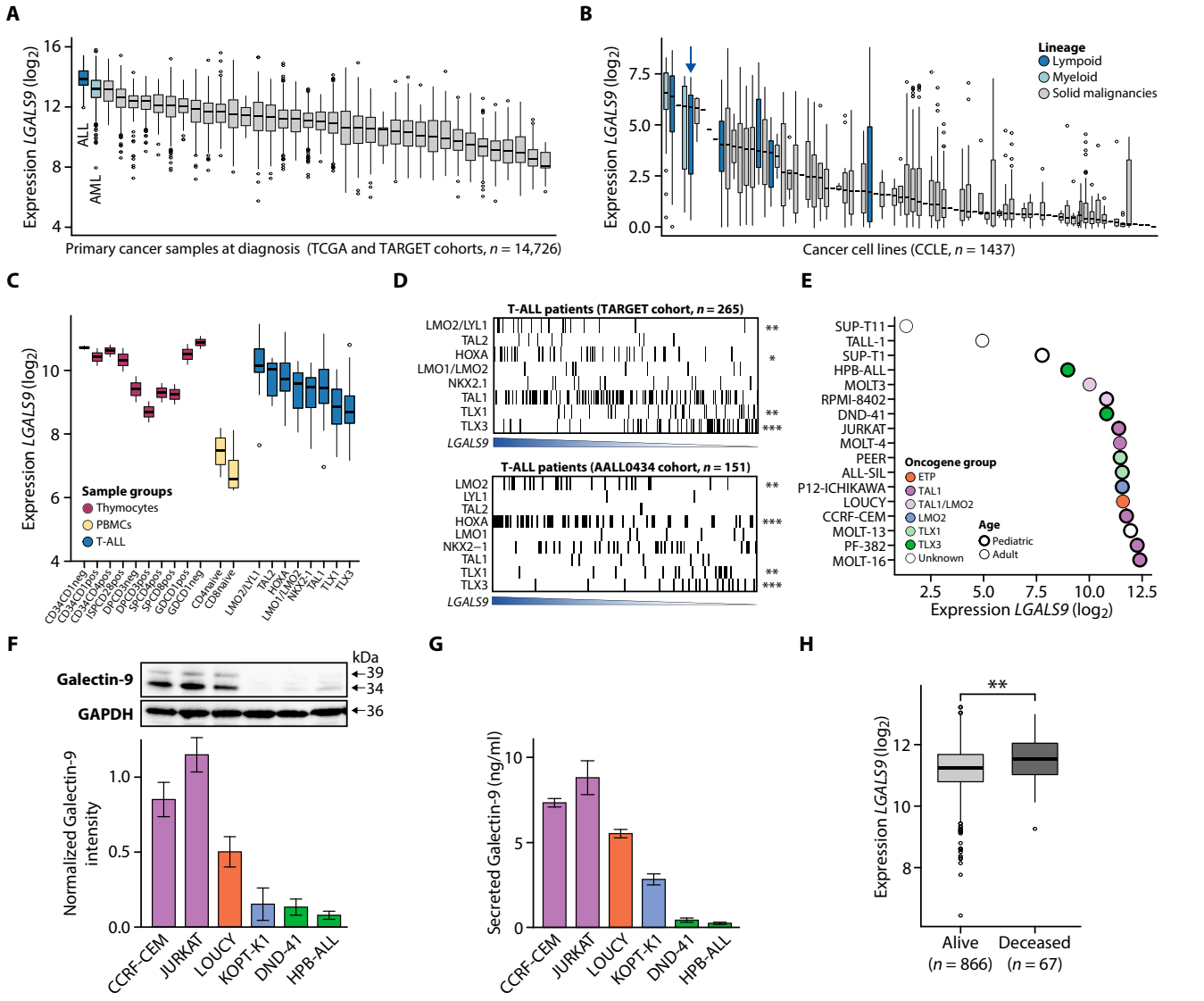

Fig. 1. Heterogeneous Galectin-9 expression in pediatric T-ALL. (**A**) Boxplots depicting $\log_2$ *LGALS9* expression (normalized count RSEM+1) in primary hematological and solid cancer samples at diagnosis in the TCGA and TARGET cohorts analyzed using the UCSC Xena platform (n = 14,726) (*20*). (**B**) Boxplots depicting $\log_2$ *LGALS9* expression (TPM+1) in hematological (colored in blue; T-ALL depicted by blue arrow) and solid (gray) cancer cell lines from the CCLE database (24Q2; n = 1437) (*21*). (**C**) Boxplots depicting $\log_2$ *LGALS9* expression (normalized DESeq2 counts+1) in healthy donor thymocytes at several differentiation stages [red, GSE151079 (*64*, *65*)], healthy donor peripheral blood CD4+ and CD8+ T cells [yellow, GSE107011 (*66*)], and in primary pediatric T-ALL patient samples at diagnosis (blue, TARGET cohort) split by T-ALL oncogenic subgroup. (**D**) Heatmap depicting oncogenic T-ALL subgroups of primary T-ALL samples sorted by *LGALS9* expression in two independent cohorts [top: TARGET (n = 265); bottom: AALL0434 (n = 151)]. Samples were split in tertiles based on *LGALS9* expression, and a Fisher exact test was used to assess enrichment of oncogenic subtypes in *LGALS9* high versus low expressing T-ALL groups. *$P < 0.05$; **$P < 0.01$; ***$P < 0.001$. (**E**) Log_2 *LGALS9* expression (normalized DESeq2 counts+1) in T-ALL cell lines [CCLE (*21*)] color coded by T-ALL subtype annotated by Squiban *et al.* (*67*). (**F**) Western blot quantification of Galectin-9 total protein levels in six T-ALL cell lines. Error bars indicate SEM of triplicates, and one representative Western blot is shown. Intensities were normalized to GAPDH and to average intensities of CCRF-CEM and Jurkat cell lines. (**G**) Bar plot showing secreted Galectin-9 in cell culture supernatant after 2 days of culture in six T-ALL cell lines assessed by ELISA. Error bars indicate SEM of triplicates. (**H**) Boxplot depicting *LGALS9* expression in pediatric patients with T-ALL from the AALL0434 cohort split by clinical outcome. **$P < 0.01$ (unpaired t test).

high Galectin-9 expressing cells at day 7. In addition, we sequenced the sgRNA plasmid library before infection and an unsorted control at day 7 to assess differences in gRNA abundance unrelated to Galectin-9 expression. We detected several sgRNAs that were depleted in the unsorted control sample compared to the validation plasmid library, suggesting that these sgRNAs targeted essential genes resulting in cell death (fig. S1C). These sgRNAs (such as *MYB*, *HSPA5*, and *FAU*) are known to be essential genes in the T-ALL cell line Jurkat according to the DepMap Chronos CRISPR database (*24*). Therefore, we removed sgRNAs that were depleted in the unsorted sample and sgRNAs targeting known essential genes (Chronos score < -1) in our further analysis as these are hits unrelated to Galectin-9 expression. Of the remaining hits, four genes, including *LGALS9* as positive control, showed more than twofold difference in

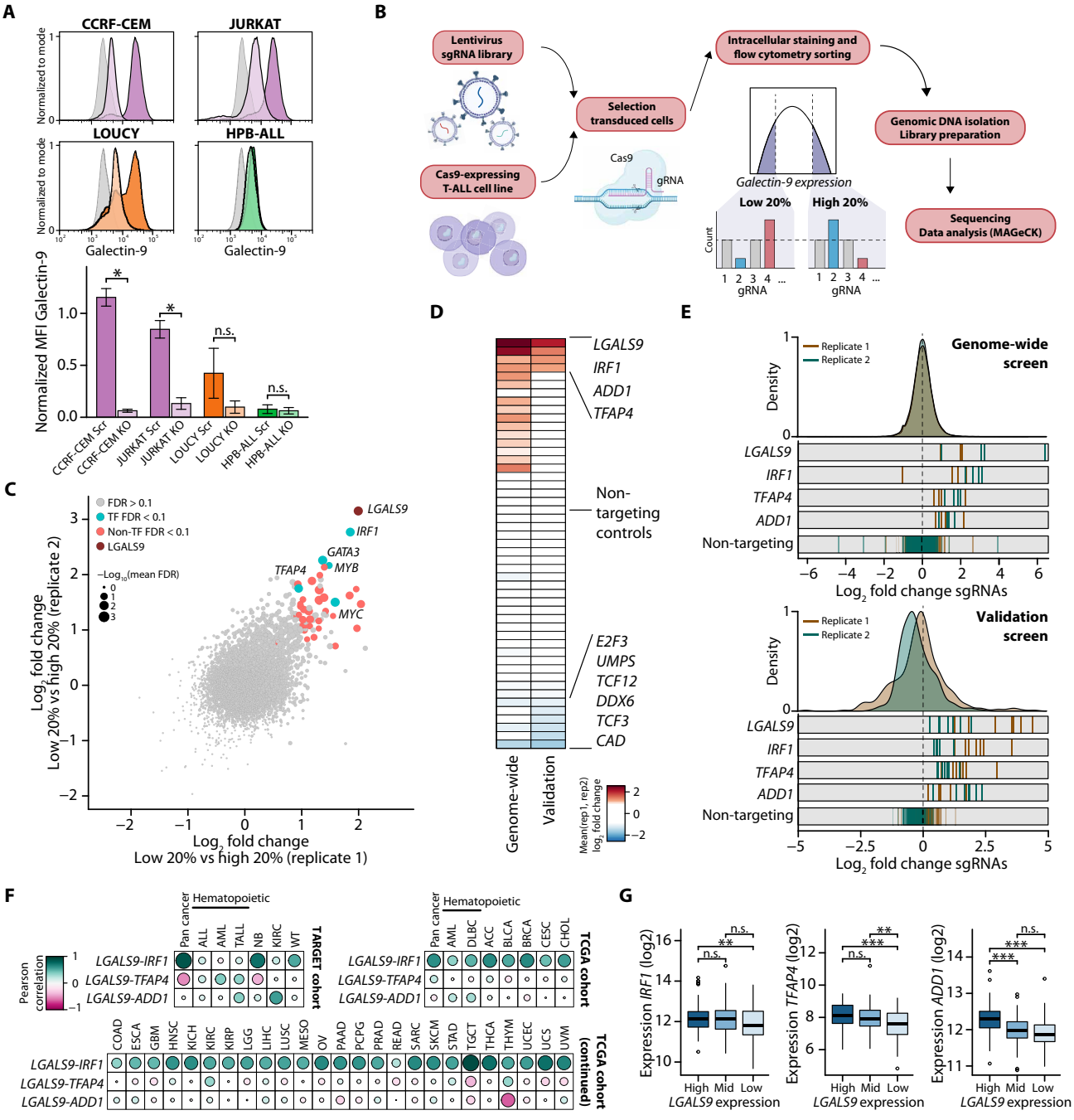

Fig. 2. Genome-wide CRISPR screen for Galectin-9 regulators in T-ALL. (**A**) Flow cytometry analysis of Galectin-9 expression in Jurkat, CCRF-CEM, Loucy, and HPB-ALL scrambled (Scr) and Galectin-9 KO T-ALL cell lines. Representative flow plots are shown (top), and the mean fluorescence intensity (MFI) was calculated of duplicate experiments (bottom) and normalized to the average MFI of Jurkat and CCRF-CEM scrambled control cell lines. A *t* test was used for statistical analysis. *$P < 0.05$; n.s., not significant. (**B**) Schematic overview of the genome-wide CRISPR screen for Galectin-9 in T-ALL cell line Jurkat. Created in BioRender. B.Y. (2025) https://BioRender.com/n03l034. (**C**) Scatterplot showing $\log_2$ fold changes of 20% low versus 20% high expressing Jurkat cells in the genome-wide CRISPR screen assessed by MAGeCK. Dot size indicates $-\log_{10}$ of the mean FDR of both replicates of a one-sided significance test using a negative binomial model by the MAGeCK algorithm (*23*). (**D**) Heatmap depicting the $\log_2$ fold change of 20% low versus 20% high Galectin-9 expressing Jurkat cells in the CRISPR genome-wide and validation screen. Only significant hits of the genome-wide screen and nontargeting controls were included and shown. (**E**) $\log_2$ fold changes of sgRNA abundance of significant hits *IRF1*, *TFAP4*, and *ADD1* and positive control *LGALS9* in the genome-wide CRISPR screen (top) and validation CRISPR screen (bottom). (**F**) Pearson correlation of *IRF1*, *TFAP4*, and *ADD1* expression with *LGALS9* expression in the TCGA and TARGET cohorts [UCSC Xena platform ($n = 14{,}726$) (*20*)]. See table S1 for abbreviations of cancer types and the number of patients. (**G**) Boxplots depicting log2 *IRF1*, *TFAP4*, and *ADD1* expression (normalized DESeq2 counts+1) in primary T-ALL (TARGET cohort, $n = 265$) split by low, mid, and high *LGALS9* expression. An unpaired *t* test was used for statistical analysis. **$P < 0.01$; ***$P < 0.001$; n.s., not significant.

sgRNA abundance between the 20% low and 20% high Galectin-9 expressing group in the validation screen, suggesting that these genes are involved in the regulation of Galectin-9 expression (Fig. 2D). These validated hits included two TFs, interferon regulatory factor 1 (*IRF1*) and TF activating enhancer binding protein 4 (*TFAP4*), and one cytoskeleton protein, adducin 1 (*ADD1*) (Fig. 2E).

Correlation of *IRF1*, *TFAP4*, and *ADD1* with *LGALS9* expression in cancer

To assess the relevance of *IRF1*, *TFAP4*, and *ADD1* in relation to *LGALS9* expression in primary cancer samples, we analyzed pan-cancer pediatric (TARGET) and adult (TCGA) cohorts using the UCSC Xena platform ($n = 14{,}726$) (*20*). Across a wide range of cancer types, *IRF1* and *ADD1* expression levels were highest in patients with ALL, whereas *TFAP4* showed intermediate expression with high variability (fig. S2A). In addition, *IRF1* expression showed a strong positive correlation with *LGALS9* expression across the pediatric pan-cancer cohort (TARGET) and adult pan cancer cohort (TCGA), as well as within each adult solid cancer type when analyzed separately (Fig. 2F and table S1). In pediatric hematologic malignancies AML and T-ALL, which are high *LGALS9* and *IRF1* expressing malignancies (Fig. 1A and fig. S2A), we detected a strong positive correlation between *LGALS9* and *TFAP4* (T-ALL and AML) and *ADD1* (T-ALL) (Fig. 2, F and G). In cancer cell lines, *IRF1* and *TFAP4* were also highly expressed in T-ALL cell lines compared to other hematologic and solid cancer cell lines (fig. S2B). Within T-ALL cell lines, *IRF1* and *TFAP4* expression were not correlated with Galectin-9 RNA and protein expression (fig. S2, C and D).

As we observed certain T-ALL oncogenic subtypes enriched in patients with T-ALL expressing low or high *LGALS9* (Fig. 1D), we sought to define how these oncogenic groups relate to the expression of our CRISPR hits. Similar to patients with T-ALL expressing low *LGALS9*, TLX1 and TLX3 subtypes were overrepresented in groups with low *IRF1*, *TFAP4*, and *ADD1* expression, although this was only significant in one of the two primary T-ALL cohorts (fig. S2, E and F). In contrast, LMO2/LYL1 subtypes were enriched in patients with high *IRF1* and *ADD1* expression, and TAL1 subtypes were enriched in patients with high *ADD1* expression in the TARGET T-ALL cohort only (fig. S2, E and F).

On the basis of our CRISPR screen hits, we postulated that the variable Galectin-9 expression is at least in part due to differential transcriptional regulation modulated by the TFs IRF1 and TFAP4. Therefore, we further focused on these two hits to unravel the epigenetic circuitry underlying Galectin-9 expression.

TFs IRF1 and TFAP4 regulate Galectin-9 expression

To further validate IRF1 and TFAP4 as transcriptional regulators of Galectin-9 expression, we generated single-cell–derived KO clones of IRF1 and TFAP4 in the two high Galectin-9 expressing pediatric T-ALL cell lines Jurkat and CCRF-CEM (fig. S3). Loss of IRF1 and TFAP4 was validated by Western blot analysis (Fig. 3A and fig. S4, A and B). Notably, IRF1 KO cell lines had significantly decreased Galectin-9 protein expression as quantified by Western blot analysis in both cell lines, at levels similar to Galectin-9 KO cell lines (Fig. 3A and fig. S4B). We also confirmed reduced Galectin-9 secretion in IRF1 KO Jurkat and CCRF-CEM T-ALL cell lines, as measured in cell culture supernatant after 2 days of culture by enzyme-linked immunosorbent assay (ELISA) (Fig. 3B and fig. S4C). KO of TFAP4 decreased Galectin-9 protein levels and secretion in Jurkat compared to scrambled controls, although to a lesser extent than IRF1 KO cells (Fig. 3, A and B). Partial TFAP4 KO in CCRF-CEM (50% indel; fig. S3) displayed an only modest decrease in Galectin-9 protein levels compared to scrambled controls (fig. S4, B and C).

Next, as IRF1 and TFAP4 exert their function as TFs, we investigated their role for transcriptional regulation of *LGALS9* expression. *LGALS9* expression as assessed by reverse transcription quantitative polymerase chain reaction (RT-qPCR) was significantly decreased in IRF1 KO Jurkat and CCRF-CEM cells (Fig. 3C and fig. S4D). *LGALS9* expression was also significantly decreased in Jurkat TFAP4 KO cell lines (Fig. 3C), but this was not significant for CCRF-CEM, possibly due to its partial KO (fig. S4D). Knocking out IRF1 in single-cell–derived TFAP4 KO Jurkat cells further decreased Galectin-9 RNA and protein expression to similar levels as IRF1 KO alone (Fig. 3, D and E). Together, these results suggest that IRF1 and TFAP4 drive and enhance Galectin-9 expression through transcriptional regulation.

As it has been described that IRF1 is responsive to IFN-γ signaling and IFN-γ treatment induced Galectin-9 secretion in the AML cell line THP-1 (*5*), we hypothesized that IRF1 may be acting downstream of IFN-γ. To this end, we investigated the effect of IFN-γ treatment on *LGALS9* expression in Jurkat and CCRF-CEM IRF1 KO and scrambled control cell lines. Although IFN-γ treatment increased *LGALS9* expression in scrambled control cells, this increase was neutralized in IRF1 KO cell lines (Fig. 3F and fig. S4E). Furthermore, it has been described that PMA increases Galectin-9 expression in Jurkat T-ALL cells (*13*). Although 24-hour treatment with PMA in Jurkat scrambled and TFAP4 KO induced an ~3.5-fold increase in *LGALS9* expression, this effect was reduced with PMA treatment in IRF1 KO cells (twofold increase; fig. S4F). These results suggest that the induction of *LGALS9* expression by IFN-γ is mediated through IRF1, but additional mechanisms may contribute to *LGALS9* expression after PMA treatment.

To validate the regulatory role of IRF1 and TFAP4 for *LGALS9* expression in primary T-ALL, we analyzed the activity of TFs by assessing regulon activity using RScenic, which is a measure for TF activity based on their target gene expression (*25*). Regulon activity of IRF1 and TFAP4 was highest in primary patient samples with high *LGALS9* expression (Fig. 3G). Regulons that were found in the same hierarchical cluster as IRF1 and TFAP4 included IRF, HOX, and STAT TF families (table S2). Together, these results suggest that IRF1 and TFAP4 play a role in regulating Galectin-9 expression on the transcriptional level in T-ALL cell lines and primary T-ALL patient samples.

IRF1 and TFAP4 bind regulatory DNA elements of *LGALS9*

As KO of IRF1 and TFAP4 decreased *LGALS9* expression, we postulated that these TFs bind regulatory DNA elements within the *LGALS9* locus to modulate its expression. We therefore analyzed histone 3 lysine 27 acetylation (H3K27ac) chromatin immunoprecipitation followed by sequencing (ChIP-seq) in six T-ALL cell lines to identify active regulatory DNA elements. We observed H3K27ac enrichment on the *LGALS9* promoter and detected several active enhancers nearby with variable H3K27ac enrichment across T-ALL cell lines (Fig. 4A). To identify which enhancers interact with the *LGALS9* promoter, we performed H3K27ac HiChIP-seq in four T-ALL cell lines (Jurkat, CCRF-CEM, Loucy, and HPB-ALL), which displayed variable enhancer landscapes and Galectin-9 expression. Notably, no enhancer looping was detected in HPB-ALL, a cell line

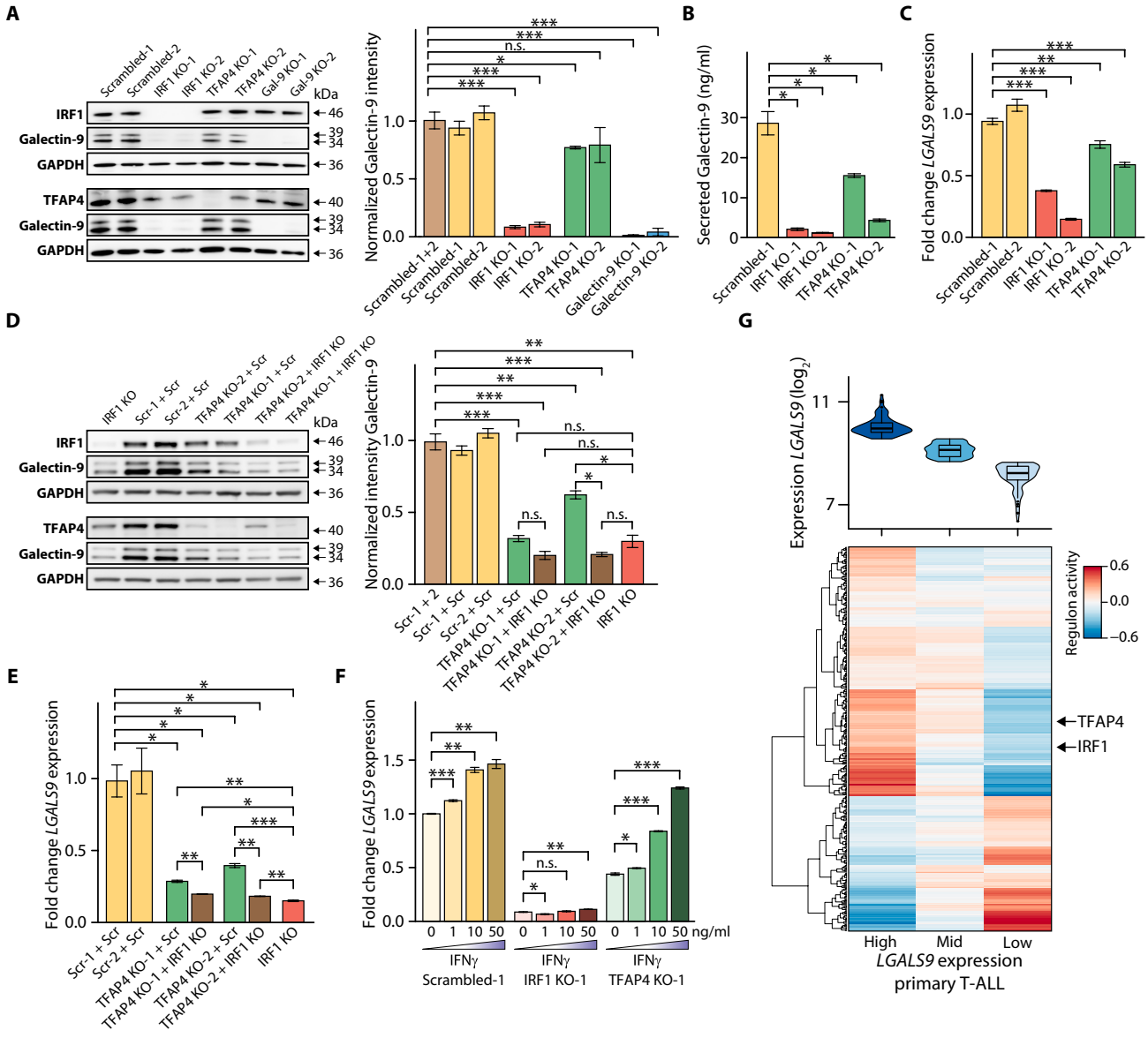

Fig. 3. TFs IRF1 and TFAP4 regulate Galectin-9 expression. (**A**) Western blot quantification in single-cell–derived CRISPR KO clones in Jurkat T-ALL cells. Intensities were normalized to GAPDH and scrambled controls. Error bars indicate SEM of duplicates for which Western blots are shown. Data of scrambled 1+2 represent both scrambled controls together. (**B**) Bar plot showing Galectin-9 concentration secreted in cell culture supernatant after 2 days of culture in Jurkat scrambled control, IRF1 KO, and TFAP4 KO cell lines. Error bars indicate SEM of triplicates. (**C**) Bar plot depicting fold change of *LGALS9* expression assessed by RT-qPCR compared to scrambled control in Jurkat scrambled, IRF1 KO, and TFAP4 KO cell lines. Error bars indicate SEM of triplicates. (**D** and **E**) Western blot (WB) quantification (D) and fold change of *LGALS9* expression assessed by RT-qPCR (E) of IRF1-TFAP4 dual KO Jurkat cells. Single-cell–derived scrambled or TFAP4 KO cell lines were subjected to CRISPR editing of IRF1 and scrambled gRNAs. A bulk IRF1 KO sample was taken along as well and note order TFAP4 KO2/1 in WB. WB intensities were normalized to GAPDH and scrambled controls. Error bars indicate SEM of duplicates (D) or triplicates (E). Data of scrambled 1+2 represent both scrambled controls together. (**F**) Bar plot depicting fold change of *LGALS9* expression assessed by RT-qPCR of Jurkat cells treated with a range of IFN-γ for 48 hours. Expression was normalized to vehicle-treated scrambled control. Error bars indicate SEM of triplicates. (**G**) Heatmap depicting TF activity analysis [RScenic (*25*)] in primary pediatric T-ALL patient samples from the TARGET cohort ($n = 265$). Samples were equally split in *LGALS9* high, mid, and low expressing groups. See table S2 for other regulons in the same hierarchical cluster as IRF1 and TFAP4. An unpaired *t* test was used for all statistical analysis. $^*P < 0.05$; $^{**}P < 0.01$; $^{***}P < 0.001$; n.s., not significant.

displaying low Galectin-9 expression (Fig. 2A and fig. S5A), whereas we observed several enhancers looping to the *LGALS9* promoter in all three cell lines that showed higher Galectin-9 expression (Fig. 4B and fig. S5A). Overall, we detected three enhancers looping to the *LGALS9* promoter in Jurkat and CCRF-CEM cells, of which one enhancer was located at the 3′ end of *LGALS9* and two enhancers were located in an intronic region of the neighboring gene *KSR1* (Fig. 4B).

To assess whether IRF1 and TFAP4 bind the *LGALS9* promoter and associated enhancers, we performed IRF1 and TFAP4 ChIP-seq in all six T-ALL cell lines. IRF1 chromatin binding was detected specifically on the *LGALS9* promoter in all T-ALL cell lines, in

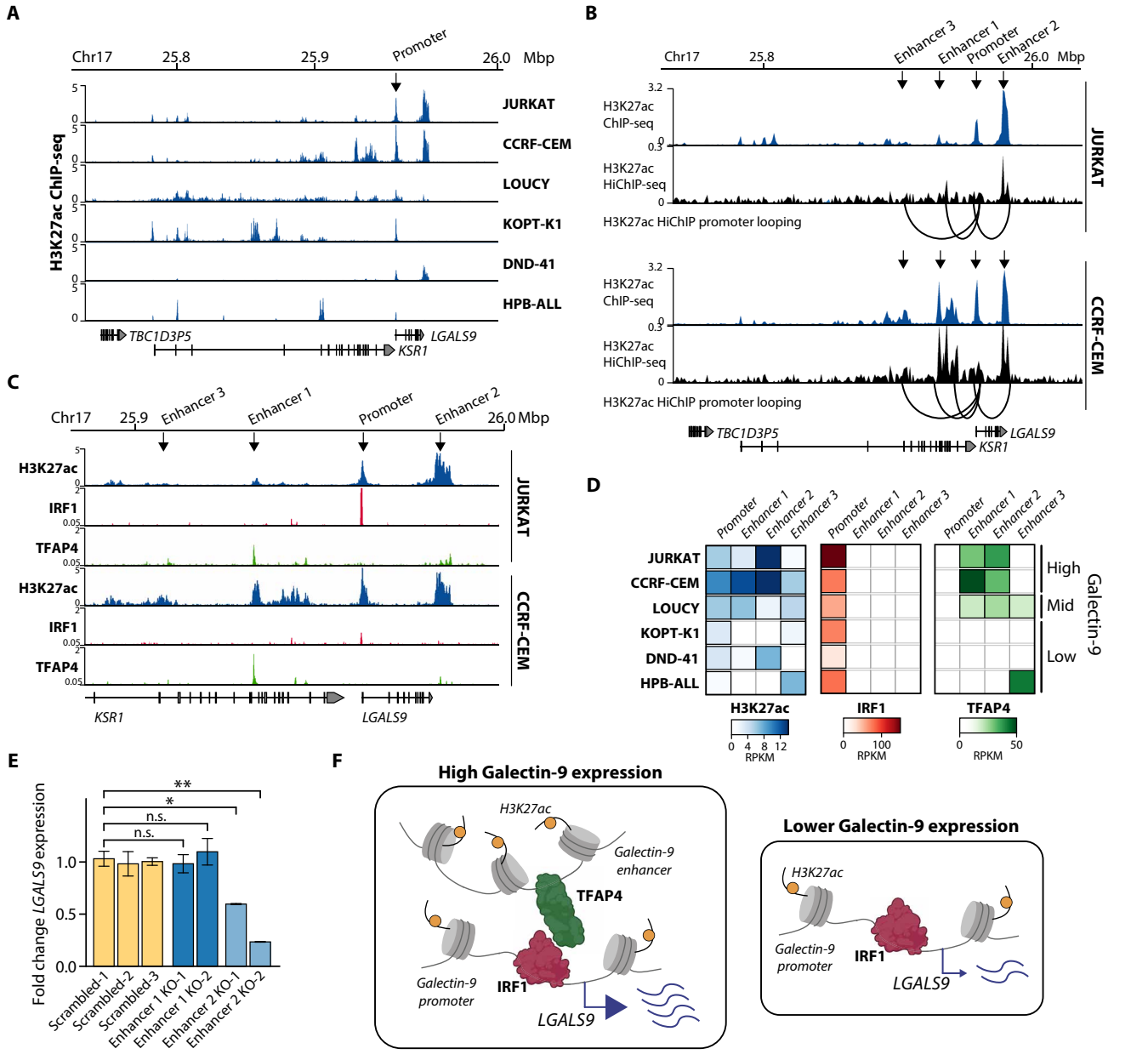

Fig. 4. IRF1 and TFAP4 bind regulatory DNA elements of *LGALS9*. (**A**) H3K27ac enrichment in the *LGALS9* locus analyzed by ChIP-seq experiments in T-ALL cell lines. (**B**) Chromatin looping analyzed by H3K27ac HiChIP-seq experiments in Jurkat and CCRF-CEM cells. Only chromatin looping from the *LGALS9* promoter is shown, and three enhancers detected in both cell lines are indicated by an arrow. (**C**) H3K27ac, IRF1, and TFAP4 enrichment in the *LGALS9* locus analyzed by ChIP-seq experiments in Jurkat and CCRF-CEM cells. (**D**) Heatmap depicting H3K27ac (left), IRF1 (middle), and TFAP4 (right) enrichment on the *LGALS9* promoter and three identified enhancers. Faint gray outline indicates that this region is not peak called in the respective sample. (**E**) Bar plot depicting fold change of *LGALS9* expression assessed by RT-qPCR compared to scrambled control in single clone–derived CRISPR-edited Jurkat cells upon a 150-bp deletion in enhancer 1, a 1.6-kb deletion in enhancer 2, or scrambled controls. Error bars indicate SEM of triplicates, and an unpaired *t* test was used for statistical analysis; $*P < 0.05$; $**P < 0.01$; n.s., not significant. (**F**) Schematic summary of the transcriptional regulation of *LGALS9* expression. Created in BioRender. B.Y. (2025) https://BioRender.com/a56h547.

contrast to TFAP4 binding that we observed only on *LGALS9* enhancers but not on the promoter (Fig. 4, C and D, and fig. S5B). Only enhancers 1 and 2 displayed high H3K27ac enrichment and TFAP4 enrichment in high Galectin-9 expressing T-ALL cell lines (Jurkat and CCRF-CEM). On the other hand, T-ALL cell lines with lower Galectin-9 expression (KOPT-K1, DND-41, and HPB-ALL) did not show any TFAP4 enrichment on these enhancers, suggesting that enhancers 1 and 2 may play a role in enhancing *LGALS9* expression in T-ALL.

Deletion of 3′ enhancer decreases *LGALS9* expression

We next sought to investigate whether deleting enhancers 1 and 2 resulted in reduced *LGALS9* expression. We designed sgRNAs surrounding the center of the H3K27ac peak and TFAP4 binding and

used the CRISPR-Cas9 system to generate deletions of the endogenous enhancers 1 and 2 (fig. S5, C and D). Single-cell–derived CRISPR enhancer deletion clones of enhancer 2 significantly decreased *LGALS9* RNA expression compared to scrambled controls as assessed by RT-qPCR; however, no significant differences were observed by deleting a 150–base pair (bp) region in enhancer 1 in single-cell–derived CRISPR-edited Jurkat cells (Fig. 4E) and in dual enhancer 2/enhancer 1 CRISPR deletions (fig. S5, E and F). Together, this suggests that specifically the TFAP4-occupied enhancer 2 increases *LGALS9* expression in T-ALL. These results are consistent with IRF1 regulating *LGALS9* expression through direct binding at its promoter and being required for strong expression in T-ALL, and TFAP4 further enhancing *LGALS9* expression through chromatin binding on a 3′ enhancer (Fig. 4F).

DISCUSSION

In this study, we employed a genome-wide CRISPR screen in T-ALL to unravel transcriptional regulators of Galectin-9 and identified IRF1 and TFAP4 as positive transcriptional regulators of *LGALS9*. We show that both TFs act through binding at DNA regulatory elements by demonstrating IRF1 binding at the *LGALS9* promoter and TFAP4 binding at a 3′ *LGALS9* enhancer.

Across cancers, *LGALS9* and *IRF1* were highly expressed in hematological malignancies, including T-ALL and AML, compared to a wide range of solid cancer types. We identified a strong positive correlation between *LGALS9* and *IRF1* expression in a pan-cancer analysis and within each solid cancer type, suggesting that IRF1 plays a critical role in regulating *LGALS9* expression in cancer in general. In T-ALL and AML, we observed a strong positive correlation between *TFAP4* and *LGALS9* expression suggesting that TFAP4 adds another layer of regulation of *LGALS9* expression in hematological malignancies with high *IRF1* expression at baseline.

Several oncogenic subtypes have been described in T-ALL, which are mostly driven by genetic rearrangements of key genes (*15*, *26*). In two independent cohorts of pediatric patients with T-ALL, we identified a significant enrichment of TLX1 and TLX3 subtypes in patients with low *LGALS9* expression, in contrast to HOXA and LMO2 subtypes, which were significantly enriched in patients with high *LGALS9* expression. The associations of T-ALL subtypes with expression of *IRF1*, *TFAP4*, and *ADD1* were less clear, being significant in only one of the two cohorts. This suggests that the observed associations between T-ALL subtypes and *LGALS9* expression cannot be solely explained by IRF1, TFAP4, or ADD1. Further studies are needed to fully understand the association of these regulators with T-ALL subtypes at high granularity and to dissect the implications of IRF1 and TFAP4 and other regulators for T-ALL disease biology.

By studying chromatin looping and TF binding through H3K27ac HiChIP-seq and ChIP-seq in T-ALL, we demonstrated binding of IRF1 on the *LGALS9* promoter and TFAP4 binding on *LGALS9* enhancers in T-ALL cell lines. Specifically, we identified IRF1 binding in all six T-ALL cell lines tested with variable Galectin-9 expression, whereas TFAP4 binding was detected only on enhancers in those T-ALL cell lines expressing mid to high Galectin-9 levels. By performing KO experiments, we identified IRF1 as being indispensable for *LGALS9* expression, whereas TFAP4 plays a role to further enhance basal expression levels of *LGALS9*.

IRF1 is expressed in multiple cell types of the innate and adaptive immune system. In hematopoietic stem cells, IRF1 has been shown to regulate self-renewal (*27*), whereas in T cells, it is required for CD8+ lineage commitment in thymocytes (*28*) and responsible for Tr1 cell differentiation (*29*). In contrast to normal immune cells where IRF1 has been associated with an inflammatory response (*27*, *30*), IRF1 in tumor cells induces an immunosuppressive environment through up-regulation of PD-L1 on solid tumor cells (*31*, *32*). Whereas IRF1 KO colon and melanoma mouse models did not show a proliferative disadvantage in vitro, IRF1 KO cells displayed lower tumorigenicity in vivo due to increased sensitivity to cytotoxic CD8+ T cells (*31*). In addition, expression of IRF1 in tumor cells has been shown to suppress IFN-induced antitumor T cell activation (*32*). Although it remains unclear whether IRF1 induces PD-L1 expression in hematologic malignancies including T-ALL, we found a role for IRF1 in sustaining strong *LGALS9* expression in T-ALL. *LGALS9* is expressed at higher basal levels than observed in solid tumors, supporting a critical role in regulating the tumor immune response. As other hematologic malignancies, such as AML, also expressed high levels compared to solid tumor types, further studies are needed to investigate whether IRF1 exerts the same function in other leukemias. Although we focused on the regulation of Galectin-9 as a dominant factor within the immune microenvironment, further studies are needed to understand the relative contributions of other immunosuppressive mediators and their interplay for T-ALL biology.

In glioma, the AKT/GSK3B-IRF1 pathway has been described to be involved in the secretion of Galectin-9, specifically upon loss of PTEN, and PTEN KO cell lines displayed higher *LGALS9* expression than PTEN wild-type cells (*33*). PTEN is frequently deleted in T-ALL (*14*, *15*), and the T-ALL cell lines Jurkat, CCRF-CEM, and Loucy, which displayed mid/high Galectin-9 expression, are PTEN-deleted cell lines (*34*, *35*). However, we also observed IRF1 binding on the *LGALS9* promoter in T-ALL cell lines with lower *LGALS9* expression, suggesting that IRF1 plays a role for *LGALS9* expression across T-ALL samples irrespective of their PTEN deletion status. Furthermore, although PMA treatment, which mimics signaling through activation of PKC, induced *LGALS9* expression in Jurkat cells, this increase was attenuated in IRF1 KO cells but not in TFAP4 KO cells. This suggests that IRF1, but not TFAP4, acts downstream of PKC to regulate *LGALS9* expression, possibly through GSK3B as PKC is also known to phosphorylate GSK3B like AKT (*36*–*38*). Exactly how the PKC pathway may contribute to IRF1 regulation in T-ALL needs to be investigated further. We also showed that IFN-γ induced expression of *LGALS9* in T-ALL is solely dependent on IRF1 as the IFN-γ induced increase in *LGALS9* was neutralized in Jurkat and CCRF-CEM IRF1 KO cells. Together, this suggests that *LGALS9* expression can be modulated by IFN-γ (through IRF1) and PKC signaling, but further studies are needed to understand the relative contributions and potential cross-talk of these signaling pathways for *LGALS9* expression.

In contrast to the key role of IRF1 in sustaining strong *LGALS9* expression in T-ALL, we also found a role for TFAP4 in fine-tuning expression of *LGALS9* by binding at one enhancer within the *LGALS9* locus in T-ALL. The function of TFAP4 as a transcriptional activator for Galectin-9 has been previously unknown. TFAP4 is a Myc target gene and is involved in various biological processes including proliferation, stemness, and tumor initiation (*39*, *40*). In adaptive immune cells, TFAP4 sustains activation and expansion of

CD8+ T cells during acute infection (*41*) and was identified as the key TF to enhance fitness of chronically activated CAR-T cells in a knock-in screen of 100 TFs (*42*). In cancer, TFAP4 has been mainly described as a key regulator of cell cycle progression (*43*–*45*). It is overexpressed in various tumor types and linked to poor prognosis (*39*, *46*). In T-ALL, TFAP4 fine-tunes *LGALS9* expression through its binding to a specific 3′ enhancer ("enhancer 2"), which we identified as a key regulatory region. The larger H3K27ac enrichment observed across enhancer 2, compared to enhancer 1, highlights its strong enhancer activity. Within enhancer 2, we identified three smaller subpeaks of H3K27ac enrichment with TFAP4 binding, suggesting that enhancer 2 functions as a composite regulatory element. The significant reduction in *LGALS9* expression upon deleting enhancer 2 further supports its role as a regulatory hub. Further studies are needed to gain deeper mechanistic insights into TFAP4 binding at this regulatory hub. The proximity of enhancer 2 to the 3′ untranslated region of the *LGALS9* gene also suggests that potential posttranscriptional mechanisms might play a role through regulating RNA stability, alternative polyadenylation, or microRNA-mediated regulation. In addition, a possible direct effect of TFAP4 on Galectin-9 secretion warrants further exploration. Together, our study suggests a role for TFAP4 in inducing an immunosuppressive microenvironment in T-ALL through transcriptional regulation of *LGALS9* expression.

Besides the TFs IRF1 and TFAP4, we also identified ADD1 as a positive regulator of Galectin-9. ADD1 is a ubiquitously expressed cytoskeleton protein and plays a role in a variety of processes including signal transduction, cell motility, proliferation, adhesion, and regulation of the membrane cytoskeleton (*47*). As we detected this hit as a positive regulator of intracellular Galectin-9 protein expression, it remains to be investigated exactly how ADD1 is involved in regulating Galectin-9 protein levels and Galectin-9 secretion in T-ALL.

The Galectin-9/Tim-3 interaction has been widely studied for its role in T cell apoptosis and dysfunction (*5*, *48*, *49*). Whereas, in some cancers, Galectin-9 exerts a pro-tumor role, in others, it has been associated with immunosuppression (*4*–*6*). Here, we demonstrate that pediatric patients with T-ALL who did not survive displayed higher *LGALS9* expression levels than those who did not, in line with prior works associating Galectin-9 expression with poor outcome (*4*–*6*). Our study suggests that down-regulating *LGALS9* expression by inhibiting IRF1 and/or TFAP4 may provide an innovative therapeutic angle in addition to direct blocking of the Galectin-9/Tim-3 interaction.

MATERIALS AND METHODS

T-ALL cell lines

T-ALL cell lines Jurkat [American Type Culture Collection (ATCC)], CCRF-CEM (ATCC), Loucy (ATCC), KOPT-K1 (kind gift of J. Aster), DND-41 (kind gift of J. Aster), and HPB-ALL (DSMZ) were maintained at 37°C and 5% CO_2 in RPMI 1640 (Thermo Fisher Scientific, no. 11875-085) with 10% of heat-inactivated fetal bovine serum (Thermo Fisher Scientific, no. 26140-079), 25 mM Hepes (Thermo Fisher Scientific, no. 15630-080), 55 nM 2-mercaptoethanol (Thermo Fisher Scientific, no. 21985-023), 1% pen/strep (Thermo Fisher Scientific, no. 15140163), 1% glutamine (Life Technologies, no. 25030164), 1% NEAA (Thermo Fisher Scientific, no. 11140-050), and 1% sodium pyruvate (Thermo Fisher Scientific, no. 11360-070). 293T cells (ATCC) were maintained at 37°C and 5% CO_2 in Dulbecco's modified Eagle's medium (Thermo Fisher Scientific, 11995-073) with 10% of heat-inactivated fetal bovine serum and 1% pen/strep. All cell lines were verified by DNA fingerprinting at the DFCI Molecular Diagnostics Core and were regularly tested for mycoplasma contamination.

CRISPR screens

Virus generation, infection, and titration

Lentivirus was generated by transfecting 293T cells in 6-mm dishes at 60% confluency with 8 μg of plasmid DNA of interest, 10 μg of psPAX2 (Addgene plasmid no. 12260), and 1 μg of VSV.G (Addgene plasmid no. 14888) in 10-μl prewarmed Opti-MEM (Thermo Fisher Scientific, no. 31985088) and 61-μl LT-1 transfection reagent (Mirus Bio, no. MIR2304). Plasmid DNA, packaging vectors, and LT-1 mixture was incubated for 30 min before adding to 293T cells. Media were changed after 6 to 8 hours, and viral supernatants were collected and filtered 36 hours posttransfection.

To determine viral titer, 1 million Jurkat cells were infected with different amounts of virus and polybrene (4 μg/ml; Santa Cruz Biotechnology, no. 31985088) in 2 ml of media by spinning at 1000*g* for 2 hours at 33°C and overnight incubation at 37°C and 5% CO_2. A total of 4000 cells were transferred into 96-well plates with and without selection antibiotics for 3 days [1 μg/ml puromycin (Sigma-Aldrich, no. 31985088)] or 10 days (4 μg/ml blasticidin (Invitrogen, no. 31985088)] depending on the antibiotic resistance gene of the plasmid. Cell viability was assessed using the CellTiter-Glo Luminescent Cell Viability Assay (Promega, no. G7572) according to protocol. Virus titer was calculated using the formula depicted as: titer (IU/ml) = (cell number × viable percentage)/(virus amount in ml) where the viable percentage represents the ratio of viable cells in samples cultured with selection antibiotics versus control samples cultured without selection antibiotics.

Cas9 activity assay

For each lentiviral-based CRISPR-Cas9 experiments performed in this study, we generated lentiviral Cas9-expressing T-ALL cell lines as T-ALL cell lines loose Cas9 activity over time. First, Jurkat cells were infected as described above with Cas9 lentivirus (lentiCas9-Blast, Addgene no. 52962) at an MOI of 0.7. To ensure high activity of Cas9 in T-ALL cell lines, we performed a Cas9 activity assay before and at the start of each CRISPR screen experiment. For detailed protocols, we refer to the Broad Institute website (https://portals.broadinstitute.org/gpp/public/resources/protocols). In short, lentiviral Cas9-expressing Jurkat cells were infected at an MOI of 1 as described above with pXPR lentivirus (pXPR_047) that contains the enhanced GFP (EGFP) open reading frame and an sgRNA against EGFP. pXPR_047 was a gift from D. Root (Addgene plasmid no. 107145). In Cas9-expressing cells, the EGFP sequence will be targeted by the sgRNA, resulting in the loss of EGFP fluorescence. After 10-day selection with blasticidin (4 μg/ml), Cas9 activity was determined by the fraction of infected, puromycin-selected cells that were EGFP negative on day 5 postinfection with pXPR_047, with >75% GFP-negative considered sufficient for CRISPR screen experiments.

Genome-wide CRISPR screen infection and sorting

Genome-wide CRISPR screening was based on the protocol previously described by Joung *et al.* (*50*). A total of 200 million lentiviral Cas9-expressing Jurkat cells, which displayed >75% GFP-negative cells in the Cas9 activity assay, were infected with the genome-wide

Brunello library lentiviral prep (Addgene no. 73178-LV) to achieve 651-fold coverage per sgRNA at an MOI of 0.25. Cells were selected with puromycin (1 μg/ml) and harvested at 7 days postinfection. Human Brunello CRISPR KO pooled library was a gift from D. Root and J. Doench (Addgene viral prep no. 73178-LV) (*22*).

A total of 100 million cells for the first replicate and 60 million cells for the second replicate were harvested at day 7 and stained with 7-AAD (Life Technologies, no. 31985088) to label dead cells. Next, cells were fixed and permeabilized with Fixation/Permeabilization buffer (BD Biosciences, no. 554714) according to protocol. For primary antibody staining, cells were incubated with 1:200 anti–Galectin-9 (Abcam, #ab227046) or immunoglobulin G (IgG) control (Abcam, no. ab172730) in BD Wash/Perm buffer at 4°C for 30 min in the dark. Cells were washed twice with 1x BD Wash/Perm buffer and stained with 1:3000 Alexa Fluor 488–conjugated secondary antibody (Abcam, no. ab150077). Cells were washed twice and sorted using a BD FACSAria II machine to collect the 20% low and 20% high Galectin-9 expressing populations (fig. S1B). Data were analyzed using FlowJo software. The same number of cells (100 million for the first screen and 60 million for the second replicate) were harvested as unsorted controls and snap frozen until further processing.

Genome-wide CRISPR screen library preparation

To assess the gRNA abundance in sorted populations, we isolated gDNA and amplified the gRNA sequence as follows. Fixed cells were de-cross-linked and lysed using tissue lysis buffer ATL (Qiagen, no. 939011) and 0.2 ml of proteinase K (Qiagen, no. 19133) overnight at 56°C. gDNA of unfixed cells or de-cross-linked cells were extracted using the QIAamp DNA Blood Midi Kit (Qiagen, no. 51183).

To amplify the gRNA region in the gDNA, we performed two PCR reactions. First, up to 2 μg of gDNA was amplified using the NEBNext High-Fidelity 2X PCR Master Mix (New England Biolabs, no. M0541L) and 0.25 μM forward (Fw) and 0.25 μM reverse (Rv) primers [PCR1_Fw and PCR1_Rv (table S3)] using the following PCR conditions: 1x (98°C for 2 min); 30x (95°C for 20 s, 60°C for 20 s, and 72°C for 30 s); 1x (72°C for 5 min). An initial 30-cycle run was conducted using an unsorted sample to confirm the presence of a single band. All gDNA from sorted samples were amplified using 12 to 20 cycles. To determine the optimal template amount, a test run with 40 cycles using varying concentrations of gDNA was performed. The gDNA concentration that produced the best results was selected. PCR products were confirmed on a 2% agarose gel.

The second PCR was performed for sample barcoding. All PCR product from the first PCR reaction was pooled, and 1 μl was used for the second PCR reaction in duplicates. One microliter of PCR 1 product was amplified using the NEBNext High-Fidelity 2X PCR Master Mix (New England Biolabs, no. M0541L) and 0.5 μM Fw and Rv primers containing DNA barcodes and a stagger region with variable lengths to increase sequence diversity (GW_PCR_2 primers; table S3). The second PCR was performed for 12 to 20 cycles, using the same PCR conditions as PCR 1, ensuring that the total number of cycles between PCR1 and PCR2 did not exceed 35 cycles. PCR products of 373 bp were gel extracted using the QIAquickGel Extract Kit (Qiagen no. 28704) and purified using AMPure beads (Beckman Coulter no. A63881) according to protocol. Quality control was performed using the Qubit fluorometer (Thermo Fisher Scientific) and TapeStation (Agilent), and samples were sequenced on an Illumina MiSeq or NextSeq500 aiming for a coverage of >100 reads per sgRNA in the library. Either 5% (MiSeq) or 20% (NextSeq500) PhiX was included to improve library diversity.

Genome-wide CRISPR screen analyses

Demultiplexed fastq files were provided as input for the "count_spaces_genome.py" script from the Zhang lab (https://github.com/fengzhanglab/Screening_Protocols_manuscript/) to count abundance of gRNAs. The MAGeCK algorithm was performed to identify differential abundance of gRNAs. gRNA read counts from the Galectin-9 20% low gates were compared against read counts in the Galectin-9 20% high gates (*23*). Significant enriched sgRNAs were tested using a negative binomial model providing one-sided *P* values using the MAGeCK algorithm. The sgRankView function from the MAGeCKFlute R package was used to visualize $\log_2$ fold changes of individual gRNAs.

The validation pool included 41 genes that were enriched in the Galectin-9 20% low gates with an FDR of <0.15 in both replicates. In addition, 38 genes with enriched abundance in the Gal9 20% high gates and an FDR of <0.15 in at least one replicate were also included. Ribosomal genes were excluded from the validation pool. For each gene, we included four gRNAs from the Brunello library (same as in the genome-wide screen) (*22*) and three different gRNAs from the Liu library resulting in a total of seven sgRNAs per gene. Human lentiviral CRISPR library was a gift from X. S. Liu (Addgene no. 1000000132). We also included 100 negative control gRNAs from the Brunello library. For each sgRNA sequence in the validation pool, the 5′ universal flanking sequence TATCTTGTGGAAAGGACGAAACACC was prepended. In addition, if an sgRNA sequence started with any nucleotide other than "G," an extra "G" was prepended to ensure efficient transcription from the U6 promoter. Then, the 3′ universal flanking sequence GTTTTAGAGCTAGAAATAGCAAGTTAAAAT was appended. The validation sgRNA pool was synthesized as an oPools Oligo Pool at Integrated DNA Technologies.

Demultiplexed fastq files of the validation screen were provided as input for the "count_spaces_genome.py" script from the Zhang lab (https://github.com/fengzhanglab/Screening_Protocols_manuscript/) to count abundance of gRNAs in the validation pool from the Brunello library and Liu library. A pseudocount of 1 was added, and reads were normalized for library size. To investigate differences in the unsorted control sample versus the validation pool library, a $\log_2$ fold change was calculated. Unexpectedly, several genes were depleted from the unsorted control sample, suggesting that these are essential genes in the T-ALL cell line Jurkat. Genes with a $\log_2$ fold change of <−1 between unsorted and validation plasmid library pool as well as genes with a DepMap Chronos essential score of <−1 were removed in further analysis. Then, the mean of the two replicates was calculated per gene (seven gRNAs per gene) and visualized using the heatmap.2 function from the gplots R package.

Validation CRISPR screen preparation

To prepare the validation screen oligo pool for viral production, we amplified the synthesized oligo pool with primers [Validation_pool_Fw and Validation_pool_Rv (table S3)] to append sequences required for cloning into the backbone LentiGuide-Puro plasmid (Addgene no. 52963). We performed four reactions with each 100 ng of the synthesized oligo pool with 0.4 μM Fw/Rv primers and Phusion High-Fidelity PCR Master Mix (Thermo Fisher Scientific, no. F531L) using the following PCR conditions: 1x (98°C for 2 min); 10x (98°C for 10 s, 60°C for 15 s, and 72°C for 45 s); 1x (72°C for 5 min). PCR products of 140 bp were extracted using the Qiagen Gel Extraction Kit (Qiagen, no. 28704), quantified using NanoDrop (Thermo Fisher Scientific) and used for Gibson Assembly cloning.

The LentiGuide-Puro vector (Addgene no. 52963) was used as the sgRNA lentiviral expressing backbone for the validation pool. We performed bacterial inoculation, and plasmid DNA was isolated from the bacterial culture using the QIAGEN Plasmid Plus Maxi Kit (Qiagen, no. 12941) according to the manufacturer's instructions. For digestion, the following reaction was assembled on ice: 1 μg of Lentiguide-Puro, 1 μl of NEBuffer 3.1, 1 μl of BsmBI v2, and water to 10 μl. The reaction was incubated at 55°C for 10 min. The reaction was run on a 1% agarose gel, and the digested vector backbone was extracted using the QIAGEN Gel Extraction Kit (Qiagen, no. 28704).

To clone the validation sgRNA pools into the backbone vector, a Gibson Assembly reaction (New England Biolabs, no. E2611S) was performed with 100 ng of digested vector LentiGuide-Puro and 1 μl of the validation pool PCR product according to protocol. One μl of the Gibson Assembly reaction product was then used for bacterial transformation using Endura Electrocompetent Cells (Bioresearch Technologies, no. 60242-1) and MicroPulser Cuvettes (Bio-Rad, no. 1652082) according to protocol. In short, bacteria were electroporated at 1.8 kV and recovered for 1 hour at 37°C in 1 ml of prewarmed Recovery Medium. Ten microliters of the transformation mixture was serially diluted on LB-ampicillin plates and incubated overnight at 30°C to estimate the total number of colony-forming units. If the transformation efficiency exceeded 20-fold of the library size and the control reaction's transformation efficiency was <1% of the insert-containing reaction, plasmid DNA was isolated from a liquid bacterial culture using a QIAGEN Plasmid Plus Maxi Kit (Qiagen, no. 12941) according to the manufacturer's instructions.

Validation CRISPR screen infection and sorting

Validation pool virus and Cas9-expressing Jurkat cells were generated and validated by the Cas9 activity assay as described before. The CRISPR validation screen was performed in duplicates. For each replicate, 40 million Cas9-expressing Jurkat cells were infected with the validation screen pool virus at an MOI of 0.25 and selected using puromycin (1 μg/ml). Ten million cells to obtain >10,000 coverage were harvested on day 7 postinfection and processed for sequencing using the same protocol as described for the genome-wide screen experiment.

CRISPR single-gene KO

Single-gene or enhancer KO T-ALL cell lines were generated using the Alt-R CRISPR-Cas9 system from Integrated DNA Technologies (Integrated DNA Technologies). gRNAs targeting LGALS9, IRF1, and TFAP4 were chosen from the Brunello CRISPR library. gRNAs targeting enhancers were designed using the IDT custom Alt-R CRISPR-Cas9 gRNA tool (https://idtdna.com/site/order/designtool/index/CRISPR_CUSTOM). The following CRISPR RNA (crRNAs) were used in this study: LGALS9 (ATTCAAGGAGGTCTCCAGGA), IRF1 (GAACTCCCTGCCAGATATCG or TCTCCCTCGACAGTCATGTG), TFAP4 (CGCATGCAGAGCATCAACGC or AGGCTCCCCGGACATCTGGG), enhancer 1 (g1: CACACCTGAGCAACGCCATA and g2: CATCCTAGAGCTAGTAACCA), enhancer 2 (g1: TCGTCTCCAAGGGACCAGGA and, g2: GTTCACACGAGGCTGACAAG), KSR1 (CTGACACGGAGATGGAGCGT), and scrambled control (AACATCTCGTTAGGGGTATC). In short, Alt-R crRNA targeting gene/locus of interest and ATTO™ 550 Alt-R tracrRNA (IDT) were mixed 1:1 at a final concentration of 44 μM and heated for 5 min at 95°C. The crRNA mix was cooled down to room temperature (RT) in the dark, and the crRNA:tracrRNA complex was incubated with 36 μM Alt-R S.p. Cas9 Nuclease V3 (Integrated DNA Technologies, no. 1081058) at a ratio of 1:1 for 20 min at RT in the dark. The complex was then added to 0.5 million cells in resuspension buffer R (Thermo Fisher Scientific, no. N1025) with final concentrations of 1.8 μM electroporation enhancer DNA (Integrated DNA Technologies, no. 1075915), 1.5 μM Cas9, and 1.8 μM crRNA:tracrRNA complex. Samples were electroporated with a Neon Transfection System (Invitrogen, no. NEON1S) with the following settings: 1600 V, 10-ms pulse width, and three pulses. Cells were immediately transferred to prewarmed media without pen/strep, and tracrRNA positive cells were sorted after 24 hours on a Sony Sorter SH800. Jurkat and CCRFCEM cell lines were single cell sorted and cultured in a round-bottom 96-well plate in prewarmed cell media to generate single-cell–derived KO clones.

To determine the percentage of KO on the genomic level, we isolated gDNA using the DNeasy Blood&Tissue kit (Qiagen, no. 69504) according to protocol. A total of 550 bp around the crRNA cut site was amplified with the 2x KAPA HiFi HotStart DNA ReadyMix (Roche, no. KK2601). The PCR product was purified using ExoSAP-IT Express PCR Product Cleanup reagent (Thermo Fisher Scientific, no. 75001) and submitted for Sanger sequencing at Genewiz from Azenta Life Sciences.

Quantification of protein and RNA expression

Quantification of Galectin-9 mRNA

For quantification of *LGALS9* expression by RT-qPCR in T-ALL cell lines, RNA was isolated using TRIzol (Thermo Fisher Scientific, no. 15596026) and RNeasy kit (Qiagen, no. 74004). RNA was reverse transcribed using the SuperScript III First-Strand Synthesis SuperMix for RT-qPCR (Invitrogen, no. 11752050) and used for qPCR experiments using the SYBRgreen MasterMix (Applied Biosystems, no. 4309155). qPCR experiments were performed in triplicates. *GAPDH* (Fw: AATCCCATCACCATCTTCCA and Rv: TGGGACTCCACGACGTACTCA) was used as a housekeeping gene control to quantify *LGALS9* (Fw: GATGCCCTTTGACCTCTGCT and Rv: GTCTGGGTAATGGGAGCCG). Galectin-9 expression was induced by 24-hour treatment with PMA (50 ng/ml; MedChemExpress, no. HY-18739) in Jurkat cells or by 48-hour treatment with IFN-γ (1, 10, and 50 ng/ml; Thermo Fisher Scientific, no. 300-02-20UG) in Jurkat and CCRF-CEM cells. A *t* test was used for all statistical analysis using the compare_means function from the ggpubr package in R.

Quantification of protein expression

To quantify total Galectin-9, IRF1, and TFAP4 protein, we performed Western blot analysis. The following antibodies were used: anti–Galectin-9 at 1:1000 (Abcam, no. ab227046), anti-IRF1 at 1:1000 (Cell Signaling Technology, no. 8478), anti-TFAP4 at 1:1000 (Proteintech, no. 12017-1-AP), anti–glyceraldehyde-3-phosphate dehydrogenase (GAPDH) at 1:2500 (Santa Cruz Biotechnology, no. sc-47724), anti-rabbit IgG HRP-linked at 1:1000 (Cell Signaling Technology antibody no. 7074), and anti-mouse IgG HRP-linked at 1:5000 (Cell Signaling Technology, no. 7076). T-ALL cell lines were lysed in radioimmunoprecipitation assay (RIPA) buffer [50 mM tris-HCl (pH 7.4), 150 mM NaCl, 1% NP-40, 0.5% sodium deoxycholate, and 0.1% SDS] supplemented with 1x Complete Protease Inhibitor (Roche). Lysed cells were centrifuged at 12,000*g* for 5 min at 4°C, and the supernatant was boiled with 4x Laemmli sample buffer (Bio-Rad) at 100°C for 5 min. Equal amounts of protein sample were run on an SDS–polyacrylamide gel electrophoresis (PAGE) NuPAGE 4 to 12% Bis-Tris Protein Gel (Thermo Fisher Scientific, NP0321BOX) and transferred to Nitrocellulose Pre-Cut Blotting

Membranes (Life Technologies, LC2000) at 120 V for 90 min. Membranes were blocked in 5% nonfat dry milk in TBS-T [20 mM tris-HCl pH 7.6, 150 mM NaCl, and 0.1% Tween 20) for 1 hour at RT and incubated with primary antibodies diluted in 5% bovine serum albumin (BSA) in TBS-T overnight at 4°C. Next, membranes were washed three times with TBS-T, incubated with HRP-conjugated secondary antibodies diluted in 5% nonfat dry milk in TBS-T for 1 hour at RT and washed three times with TBS-T before detection. Protein bands were detected using SuperSignal West Pico Chemiluminescent Substrate (Thermo Fisher Scientific, no. 34577) and visualized using a ChemiDoc imaging system. Band intensities were quantified using ImageJ software (NIH), and the short and long isoforms of Galectin-9 were quantified together.

To quantify secreted Galectin-9 in the supernatant of cultured cells, we cultured T-ALL cell lines for 2 days, after which the supernatant was collected and filtered (polyvinylidene difluoride membrane, 0.45 μM). We analyzed Galectin-9 in 5x diluted supernatant (Jurkat and CCRF-CEM), 2x diluted (KOPT-K1, Loucy, DND-41), or undiluted (HPB-ALL) in triplicates using the Human Galectin-9 ELISA Kit (Abcam #ab213786) according to protocol. A *t* test was used for all statistical analysis using the compare_means function from the ggpubr package in R.

Chromatin immunoprecipitation

Chromatin immunoprecipitation sequencing

To identify IRF1 and TFAP4 binding on DNA regulatory elements in T-ALL cell lines, we performed IRF1 and TFAP4 ChIP-seq in six T-ALL cell lines (Jurkat, CCRF-CEM, Loucy, KOPT-K1, DND-41, and HPB-ALL). In addition, we performed H3K27ac ChIP-seq in the T-ALL cell line HPB-ALL. A total of 20 million cells (TF ChIP) or 4 million cells (H3K27ac ChIP-seq) were harvested and cross-linked with 1% formaldehyde for 15 min at RT with rotation, followed by quenching with 0.125 M glycine for 5 min at RT. Cells were washed twice with cold phosphate-buffered saline (PBS), lysed for 10 min on ice in lysis buffer [50 mM Hepes (pH 8.0), 140 mM NaCl, 1 mM EDTA, 10% glycerol, 0.5% NP-40, and 0.25% Triton X-100], washed twice in wash buffer [10 mM tris-HCl (pH 8.0), 200 mM NaCl, 1 mM EDTA, and 0.5 mM EGTA], and resuspended in sonication buffer [1% SDS, 10 mM EDTA, and 50 mM tris-HCl (pH 8.0)]. Complete protease inhibitor cocktail (Roche) was added fresh to all buffers. Cells were then sonicated to an average size of 200 to 500 bp using a Covaris S220 sonicator with the following parameters: peak intensity, 140; cycles/burst, 200; duty factor, 5; and 10 cycles with 60-s on/30-s off. Samples were centrifuged at maximum speed for 10 min at 4°C to remove cell debris. A whole-cell extract control was taken and stored at −20°C until reverse cross-linking.

For immunoprecipitation, the supernatant was diluted 1:1 with ChIP dilution buffer containing fresh protease inhibitors [0.01% SDS, 1.1% Triton X-100, 1.2 mM EDTA, 16.7 mM Tris (pH 8.0), and 167 mM NaCl] and incubated overnight at 4°C with IRF1 (Cell Signaling Technology, no. 8478) or TFAP4 (Sigma-Aldrich, no. HPA001912) antibodies at a 1/50 concentration. Protein A/G Dynabeads (Life Technologies, nos. 10001D and 10009D) were blocked with ChIP blocking buffer (0.5% Tween 20 and 0.5% BSA in PBS) for 1 hour at 4°C and then incubated with the chromatin-antibody mixture for 4 hours at 4°C with rotation. The beads were washed sequentially with RIPA low salt buffer [0.1% SDS, 1% Triton X-100, 1 mM EDTA, 20 mM tris-HCl (pH 8.0), 140 mM NaCl, and 0.1% sodium deoxycholate], RIPA high salt buffer (RIPA with 500 mM NaCl), LiCl buffer [250 mM LiCl, 0.5% NP-40, 0.5% sodium deoxycholate, 1 mM EDTA, and 10 mM Tris (pH 8.0)], and TE buffer. Beads were resuspended in 50 μl of ChIP elution buffer [10 mM Tris (pH 8.0), 5 mM EDTA, 300 mM NaCl, and 0.1% SDS] containing fresh 5 mM dithiothreitol. Next, 8 μl of reverse cross-linking buffer [250 mM Tris (pH 7.5), 1.25 M NaCl, 62.5 mM EDTA, and RNAse A (0.0625 mg/ml; Life Technologies, no. EN0531)] and 16 μl of Proteinase K (Qiagen, no. 19133) were added to immunoprecipitated chromatin and whole-cell extract control samples followed by incubation at 65°C for 4 hours to elute and reverse cross-link. DNA was purified using 2x Ampure (Beckman Coulter, no. A63881) bead clean-up (after removal of protein A/G beads in immunoprecipitated sample), washed twice with 80% ethanol, and eluted in Qiagen EB buffer.

For library preparation, DNA end-repair was carried out using the End-It DNA End-Repair Kit (Lucigen, no. ER0720) according to protocol. Purified DNA by AMPure beads were used for A-tailing using 10x Klenow Buffer (NEBuffer 2; NEB no. B7002S), 1 mM deoxyadenosine triphosphate (dATP), and Klenow (3′-5′ exo 5 U/μl, NEB no. M0212L) and incubated for 30 min at 37°C followed by AMPure purification. Adapter ligation was performed using the Quick Ligation Kit (NEB no. M2200S) and barcodes for each sample. Ligated products were purified by AMPure and amplified with PFU Ultra II HS (Agilent) and 0.25 μM Fw/Rv indexed primers using the following PCR program: initial denaturation at 95°C for 2 min, followed by 14 cycles of 95°C for 30 s, 55°C for 30 s, and 72°C for 30 s, with a final extension at 72°C for 1 min. The amplified DNA was size selected using AMPure beads and quantified using a Qubit fluorometer (Thermo Fisher Scientific) and Agilent TapeStation. ChIP-seq libraries were sequenced paired-end (2x37 bp) on a NextSeq500.

ChIP-seq analyses

To assess active promoters and enhancers in T-ALL cell lines, we downloaded publicly available H3K27ac ChIP-seq data: DND-41 (GSE54379), Jurkat (GSE68976), Loucy (GSE96242), KOPT-K1, and CCRF-CEM (GSE76783). The nextflow (*51*) nf-core chipseq (1.0.0.) pipeline was used to analyze ChIP-seq experiments. Default parameters were used, with hg19 as the reference genome. Narrowpeaks (IRF1: *P* value cutoff 0.0005, TFAP4 default settings) or broadpeaks were called by MACS2 (*52*) for TF or H3K27ac ChIP-seq experiments, respectively. ChIP-seq tracks were visualized in IGV Genome Browser (*53*). Read counts in peaks were counted using featureCounts (*54*) and normalized to RPKM using the rpkm() function from edgeR R package (*55*). Heatmaps were generated using the heatmap.2 function from gplots in R.

H3K27ac HiChIP-seq

H3K27ac HiChiP was performed according to protocol by Mumbach *et al.* (*56*, *57*). In short, 10 million cells were fixed as described for ChIP-seq experiments above. Then, cells were lysed and subjected to restriction digest using MBo I. Restriction overhangs were filled and marked with biotin-dATP (Thermo Fisher Scientific, no. 19524016) and dCTP (deoxycytidine triphosphate), dGTP (deoxyguanosine triphosphate), and dTTP (deoxythymidine triphosphate) and ligated with T4 DNA ligase (NEB, M0202) overnight at RT. Nuclei were then subjected to sonication using duty cycle 5, PIP 140, and cycles/burst 200 for 10 min. Clarified supernatant (1 hour at 4°C with washed protein A beads) was subjected to immunoprecipitation with 7.5 μg of anti-H3K27ac (Abcam, no. ab4729) overnight at 4°C while rotating. Next, 60 μl of washed protein A beads was added and rotated for 2 hours at 4°C. Following immunoprecipitation, DNA

was taken into biotin capture, Tn5 transposition, and library preparation as described by Mumbach *et al.* (*56*, *57*). The amplified DNA was purified using AMPure beads and quantified using a Qubit fluorometer (Thermo Fisher Scientific) and Agilent TapeStation. HiChIP-seq libraries were sequenced paired-end (2x37 bp) on a NextSeq500.

H3K27ac HiChIP-seq analysis

To analyze HiChIP-seq sequencing results, paired-end sequencing reads were trimmed using trimmomatic.0.36 and subsequently processed by HiC-Pro 2.10.0 (*58*) (reference genome hg19) with default settings. HiChIP matrices and bam files were generated using HiC-Explorer 3.4.1. (*59*, *60*). Normalized bigwigs were generated by bamCoverage from deeptools 3.0.2 (*61*)., HiChIP-seq peaks were called by hichip-peaks 0.1.2. (*62*) and HiChIP loops by the hichipper 0.7.7. algorithm (*63*). *P* value cutoffs of filtered links for visualization were 0.05 (HPB-ALL and Jurkat), 0.1 (Loucy), or 0.005 (CCRF-CEM), and only links from the *LGALS9* promoter are shown.

Primary cancer sample analyses

Gene expression

Publicly available bulk RNA sequencing (RNA-seq) data of primary T-ALL samples [TARGET initiative (https://ocg.cancer.gov/programs/target/projects/acute-lymphoblastic-leukemia), T-ALL cell lines [CCLE 24Q2; $n = 1437$ (*21*), https://sites.broadinstitute.org/ccle/], thymocytes from healthy donors (*64*, *65*), and T cells from peripheral blood healthy donors [GSE107011 (*66*)] were downloaded. TARGET data used for this analysis are available at the Genomic Data Commons (https://portal.gdc.cancer.gov). HTseq counts were normalized using DEseq2 and $\log_2$ transformed. We also downloaded normalized expression data and fusion gene data of a second primary T-ALL cohort [COG AALL0434, Gabriella Miller Kids First Pediatric Research Program ($n = 933$), accessed from the Kids First Data Resource Portal (https://kidsfirstdrc.org/) and dbGaP (https://ncbi.nlm.nih.gov/projects/gap/cgi-bin/study.cgi?study_id=phs002276.v2.p1)]. To assess enrichment and depletion of oncogenic subtypes, samples were split in tertiles based on *LGALS9* expression, and a Fisher exact test was used to assess enrichment of oncogenic subtypes in *LGALS9* high versus low expressing T-ALL groups. For analysis across cancer types, we downloaded normalized expression data of primary cancer samples at initial diagnosis from TCGA and TARGET cohorts using the UCSC Xena platform (https://xenabrowser.net/) ($n = 14{,}726$) (*20*). Pearson correlation of expression was calculated using the cor() function in R and was visualized using the corrplot function in R.

TF activity analysis

To analyze TF activity analysis (i.e., regulon activity) in bulk RNA-seq of primary T-ALL samples, we downloaded publicly available htseq counts of 265 pediatric patients with T-ALL from the TARGET initiative (https://ocg.cancer.gov/programs/target/projects/acute-lymphoblastic-leukemia). We applied RScenic (*25*) to analyze regulon activity in these 265 samples, which were divided equally in three groups based on *LGALS9* expression to assess differential regulon activity.

Supplementary Materials

The PDF file includes:

Figs. S1 to S5

Legends for tables S1 to S3

Other Supplementary Material for this manuscript includes the following:

Tables S1 to S3

REFERENCES AND NOTES

1. J. Wada, Y. S. Kanwar, Identification and characterization of Galectin-9, a novel β-galactoside-binding mammalian lectin. *J. Biol. Chem.* **272**, 6078–6086 (1997).
2. R.-Y. Yang, G. A. Rabinovich, F.-T. Liu, Galectins: Structure, function and therapeutic potential. *Expert Rev. Mol. Med.* **10**, e17 (2008).
3. N.-I. Kapetanakis, P. Busson, Galectins as pivotal components in oncogenesis and immune exclusion in human malignancies. *Front. Immunol.* **14**, 1145268 (2023).
4. M. Zhang, C. Liu, Y. Li, H. Li, W. Zhang, J. Liu, L. Wang, C. Sun, Galectin-9 in cancer therapy: From immune checkpoint ligand to promising therapeutic target. *Front. Cell Dev. Biol.* **11**, 1332205 (2024).
5. R. Yang, L. Sun, C.-F. Li, Y.-H. Wang, J. Yao, H. Li, M. Yan, W.-C. Chang, J.-M. Hsu, J.-H. Cha, J. L. Hsu, C.-W. Chou, X. Sun, Y. Deng, C.-K. Chou, D. Yu, M.-C. Hung, Galectin-9 interacts with PD-1 and TIM-3 to regulate T cell death and is a target for cancer immunotherapy. *Nat. Commun.* **12**, 832 (2021).
6. P. Dama, M. Tang, N. Fulton, J. Kline, H. Liu, Gal9/Tim-3 expression level is higher in AML patients who fail chemotherapy. *J. Immunother. Cancer* **7**, 175 (2019).
7. C. Zhu, A. C. Anderson, A. Schubart, H. Xiong, J. Imitola, S. J. Khoury, X. X. Zheng, T. B. Strom, V. K. Kuchroo, The Tim-3 ligand galectin-9 negatively regulates T helper type 1 immunity. *Nat. Immunol.* **6**, 1245–1252 (2005).
8. C. Wu, T. Thalhamer, R. F. Franca, S. Xiao, C. Wang, C. Hotta, C. Zhu, M. Hirashima, A. C. Anderson, V. K. Kuchroo, Galectin-9-CD44 interaction enhances stability and function of adaptive regulatory T cells. *Immunity* **41**, 270–282 (2014).
9. Y. Lv, X. Ma, Y. Ma, Y. du, J. Feng, A new emerging target in cancer immunotherapy: Galectin-9 (LGALS9). *Genes Dis.* **10**, 2366–2382 (2023).
10. I. M. Yasinska, N. H. Meyer, S. Schlichtner, R. Hussain, G. Siligardi, M. Casely-Hayford, W. Fiedler, J. Wellbrock, C. Desmet, L. Calzolai, L. Varani, S. M. Berger, U. Raap, B. F. Gibbs, E. Fasler-Kan, V. V. Sumbayev, Ligand-receptor interactions of Galectin-9 and VISTA suppress human T lymphocyte cytotoxic activity. *Front. Immunol.* **11**, 580557 (2020).
11. P. Anand, A. Guillaumet-Adkins, V. Dimitrova, H. Yun, Y. Drier, N. Sotudeh, A. Rogers, M. M. Ouseph, M. Nair, S. Potdar, R. Isenhart, J. A. Kloeber, T. Vijaykumar, L. Niu, T. Vincent, G. Guo, J. Frede, M. H. Harris, A. E. Place, L. B. Silverman, D. T. Teachey, A. A. Lane, D. J. DeAngelo, J. C. Aster, B. E. Bernstein, J. G. Lohr, B. Knoechel, Single-cell RNA-seq reveals developmental plasticity with coexisting oncogenic states and immune evasion programs in ETP-ALL. *Blood* **137**, 2463–2480 (2021).
12. I. Gonçalves Silva, I. M. Yasinska, S. S. Sakhnevych, W. Fiedler, J. Wellbrock, M. Bardelli, L. Varani, R. Hussain, G. Siligardi, G. Ceccone, S. M. Berger, Y. A. Ushkaryov, B. F. Gibbs, E. Fasler-Kan, V. V. Sumbayev, The Tim-3-galectin-9 secretory pathway is involved in the immune escape of human acute myeloid leukemia cells. *EBioMedicine* **22**, 44–57 (2017).
13. S. Chabot, Y. Kashio, M. Seki, Y. Shirato, K. Nakamura, N. Nishi, T. Nakamura, R. Matsumoto, M. Hirashima, Regulation of galectin-9 expression and release in Jurkat T cell line cells. *Glycobiology* **12**, 111–118 (2002).
14. S. W. Brady, K. G. Roberts, Z. Gu, L. Shi, S. Pounds, D. Pei, C. Cheng, Y. Dai, M. Devidas, C. Qu, A. N. Hill, D. Payne-Turner, X. Ma, I. Iacobucci, P. Baviskar, L. Wei, S. Arunachalam, K. Hagiwara, Y. Liu, D. A. Flasch, Y. Liu, M. Parker, X. Chen, A. H. Elsayed, O. Pathak, Y. Li, Y. Fan, J. R. Michael, M. Rusch, M. R. Wilkinson, S. Foy, D. J. Hedges, S. Newman, X. Zhou, J. Wang, C. Reilly, E. Sioson, S. V. Rice, V. Pastor Loyola, G. Wu, E. Rampersaud, S. C. Reshmi, J. Gastier-Foster, J. M. Guidry Auvil, P. Gesuwan, M. A. Smith, N. Winick, A. J. Carroll, N. A. Heerema, R. C. Harvey, C. L. Willman, E. Larsen, E. A. Raetz, M. J. Borowitz, B. L. Wood, W. L. Carroll, P. A. Zweidler-McKay, K. R. Rabin, L. A. Mattano, K. W. Maloney, S. S. Winter, M. J. Burke, W. Salzer, K. P. Dunsmore, A. L. Angiolillo, K. R. Crews, J. R. Downing, S. Jeha, C. H. Pui, W. E. Evans, J. J. Yang, M. V. Relling, D. S. Gerhard, M. L. Loh, S. P. Hunger, J. Zhang, C. G. Mullighan, The genomic landscape of pediatric acute lymphoblastic leukemia. *Nat. Genet.* **54**, 1376–1389 (2022).
15. Y. Liu, J. Easton, Y. Shao, J. Maciaszek, Z. Wang, M. R. Wilkinson, K. McCastlain, M. Edmonson, S. B. Pounds, L. Shi, X. Zhou, X. Ma, E. Sioson, Y. Li, M. Rusch, P. Gupta, D. Pei, C. Cheng, M. A. Smith, J. M. Guidry Auvil, D. S. Gerhard, M. V. Relling, N. J. Winick, A. J. Carroll, N. A. Heerema, E. Raetz, M. Devidas, C. L. Willman, R. C. Harvey, W. L. Carroll, K. P. Dunsmore, S. S. Winter, B. L. Wood, B. P. Sorrentino, J. R. Downing, M. L. Loh, S. P. Hunger, J. Zhang, C. G. Mullighan, The genomic landscape of pediatric and young adult T-lineage acute lymphoblastic leukemia. *Nat. Genet.* **49**, 1211–1218 (2017).
16. F. Gianni, L. Belver, A. Ferrando, The genetics and mechanisms of T-cell acute lymphoblastic leukemia. *Cold Spring Harb. Perspect. Med.* **10**, a035246 (2020).
17. S. S. Winter, K. P. Dunsmore, M. Devidas, B. L. Wood, N. Esiashvili, Z. Chen, N. Eisenberg, N. Briegel, R. J. Hayashi, J. M. Gastier-Foster, A. J. Carroll, N. A. Heerema, B. L. Asselin, P. S. Gaynon, M. J. Borowitz, M. L. Loh, K. R. Rabin, E. A. Raetz, P. A. Zweidler-Mckay, N. J. Winick, W. L. Carroll, S. P. Hunger, Improved survival for children and young adults with T-lineage acute lymphoblastic leukemia: Results from the children's oncology group AALL0434 methotrexate randomization. *J. Clin. Oncol.* **36**, 2926–2934 (2018).

18. D. T. Teachey, M. Devidas, B. L. Wood, Z. Chen, R. J. Hayashi, M. L. Hermiston, R. D. Annett, J. H. Archer, B. L. Asselin, K. J. August, S. Y. Cho, K. P. Dunsmore, B. T. Fisher, J. L. Freedman, P. J. Galardy, P. Harker-Murray, T. M. Horton, A. I. Jaju, A. Lam, Y. H. Messinger, R. R. Miles, M. Okada, S. I. Patel, E. S. Schafer, T. Schechter, N. Singh, A. C. Steele, M. L. Sulis, S. L. Vargas, S. S. Winter, C. Wood, P. Zweidler-McKay, C. M. Bollard, M. L. Loh, S. P. Hunger, E. A. Raetz, Children's Oncology Group Trial AALL1231: A phase III clinical trial testing bortezomib in newly diagnosed T-cell acute lymphoblastic leukemia and lymphoma. *J. Clin. Oncol.* **40**, 2106–2118 (2022).
19. B. L. Wood, M. Devidas, R. J. Summers, Z. Chen, B. Asselin, K. R. Rabin, P. A. Zweidler-Mc Kay, N. J. Winick, M. J. Borowitz, W. L. Carroll, E. A. Raetz, M. L. Loh, S. P. Hunger, K. P. Dunsmore, D. T. Teachey, S. S. Winter, Prognostic significance of ETP phenotype and minimal residual disease in T-ALL: A Children's Oncology Group Study. *Blood* **142**, 2069–2078 (2023).
20. M. J. Goldman, B. Craft, M. Hastie, K. Repečka, F. McDade, A. Kamath, A. Banerjee, Y. Luo, D. Rogers, A. N. Brooks, J. Zhu, D. Haussler, Visualizing and interpreting cancer genomics data via the Xena platform. *Nat. Biotechnol.* **38**, 675–678 (2020).
21. J. Barretina, G. Caponigro, N. Stransky, K. Venkatesan, A. A. Margolin, S. Kim, C. J. Wilson, J. Lehár, G. V. Kryukov, D. Sonkin, A. Reddy, M. Liu, L. Murray, M. F. Berger, J. E. Monahan, P. Morais, J. Meltzer, A. Korejwa, J. Jané-Valbuena, F. A. Mapa, J. Thibault, E. Bric-Furlong, P. Raman, A. Shipway, L. A. Garraway, The Cancer Cell Line Encyclopedia enables predictive modelling of anticancer drug sensitivity. *Nature* **483**, 603–607 (2012).
22. J. G. Doench, N. Fusi, M. Sullender, M. Hegde, E. W. Vaimberg, K. F. Donovan, I. Smith, Z. Tothova, C. Wilen, R. Orchard, H. W. Virgin, J. Listgarten, D. E. Root, Optimized sgRNA design to maximize activity and minimize off-target effects of CRISPR-Cas9. *Nat. Biotechnol.* **34**, 184–191 (2016).
23. W. Li, H. Xu, T. Xiao, L. Cong, M. I. Love, F. Zhang, R. A. Irizarry, J. S. Liu, M. Brown, X. S. Liu, MAGeCK enables robust identification of essential genes from genome-scale CRISPR/Cas9 knockout screens. *Genome Biol.* **15**, 554 (2014).
24. J. M. Dempster, I. Boyle, F. Vazquez, D. E. Root, J. S. Boehm, W. C. Hahn, A. Tsherniak, J. M. McFarland, Chronos: A cell population dynamics model of CRISPR experiments that improves inference of gene fitness effects. *Genome Biol.* **22**, 343 (2021).
25. S. Aibar, C. B. González-Blas, T. Moerman, V. A. Huynh-Thu, H. Imrichova, G. Hulselmans, F. Rambow, J. C. Marine, P. Geurts, J. Aerts, J. van den Oord, Z. K. Atak, J. Wouters, S. Aerts, SCENIC: Single-cell regulatory network inference and clustering. *Nat. Methods* **14**, 1083–1086 (2017).
26. P. Pölönen, D. di Giacomo, A. E. Seffernick, A. Elsayed, S. Kimura, F. Benini, L. E. Montefiori, B. L. Wood, J. Xu, C. Chen, Z. Cheng, H. Newman, J. Myers, I. Iacobucci, E. Li, J. Sussman, D. Hedges, Y. Hui, C. Diorio, L. Uppuluri, D. Frank, Y. Fan, Y. Chang, S. Meshinchi, R. Ries, R. Shraim, A. Li, K. M. Bernt, M. Devidas, S. S. Winter, K. P. Dunsmore, H. Inaba, W. L. Carroll, N. C. Ramirez, A. H. Phillips, R. W. Kriwacki, J. J. Yang, T. L. Vincent, Y. Zhao, P. S. Ghate, J. Wang, C. Reilly, X. Zhou, M. A. Sanders, J. Takita, M. Kato, N. Takasugi, B. H. Chang, R. D. Press, M. Loh, E. Rampersaud, E. Raetz, S. P. Hunger, K. Tan, T. C. Chang, G. Wu, S. B. Pounds, C. G. Mullighan, D. T. Teachey, The genomic basis of childhood T-lineage acute lymphoblastic leukaemia. *Nature* **632**, 1082–1091 (2024).
27. A. J. S. Rundberg Nilsson, H. Xian, S. Shalapour, J. Cammenga, M. Karin, IRF1 regulates self-renewal and stress responsiveness to support hematopoietic stem cell maintenance. *Sci. Adv.* **9**, eadg5391 (2023).
28. J. M. Penninger, C. Sirard, H. W. Mittrücker, A. Chidgey, I. Kozieradzki, M. Nghiem, A. Hakem, T. Kimura, E. Timms, R. Boyd, T. Taniguchi, T. Matsuyama, T. W. Mak, The interferon regulatory transcription factor IRF-1 controls positive and negative selection of $CD8^+$ thymocytes. *Immunity* **7**, 243–254 (1997).
29. K. Karwacz, E. R. Miraldi, M. Pokrovskii, A. Madi, N. Yosef, I. Wortman, X. Chen, A. Watters, N. Carriero, A. Awasthi, A. Regev, R. Bonneau, D. Littman, V. K. Kuchroo, Critical role of IRF1 and BATF in forming chromatin landscape during type 1 regulatory cell differentiation. *Nat. Immunol.* **18**, 412–421 (2017).
30. H. Feng, Y.-B. Zhang, J.-F. Gui, S. M. Lemon, D. Yamane, Interferon regulatory factor 1 (IRF1) and anti-pathogen innate immune responses. *PLOS Pathog.* **17**, e1009220 (2021).
31. L. Shao, W. Hou, N. E. Scharping, F. P. Vendetti, R. Srivastava, C. N. Roy, A. V. Menk, Y. Wang, J. M. Chauvin, P. Karukonda, S. H. Thorne, V. Hornung, H. M. Zarour, C. J. Bakkenist, G. M. Delgoffe, S. N. Sarkar, IRF1 inhibits antitumor immunity through the upregulation of PD-L1 in the tumor cell. *Cancer Immunol. Res.* **7**, 1258–1266 (2019).
32. P. K. Purbey, J. Seo, M. K. Paul, K. S. Iwamoto, A. E. Daly, A. C. Feng, A. S. Champhekar, J. Langerman, K. M. Campbell, D. Schaue, W. H. McBride, S. M. Dubinett, A. Ribas, S. T. Smale, P. O. Scumpia, Opposing tumor-cell-intrinsic and -extrinsic roles of the IRF1 transcription factor in antitumor immunity. *Cell Rep.* **43**, 114289 (2024).
33. X. Ni, W. Wu, X. Sun, J. Ma, Z. Yu, X. He, J. Cheng, P. Xu, H. Liu, T. Shang, S. Xi, J. Wang, J. Zhang, Z. Chen, Interrogating glioma-M2 macrophage interactions identifies Gal-9/Tim-3 as a viable target against *PTEN*-null glioblastoma. *Sci. Adv.* **8**, eabl5165 (2022).
34. C. Shepherd, L. Banerjee, C. W. Cheung, M. R. Mansour, S. Jenkinson, R. E. Gale, A. Khwaja, PI3K/mTOR inhibition upregulates NOTCH-MYC signalling leading to an impaired cytotoxic response. *Leukemia* **27**, 650–660 (2013).
35. H. Yuzugullu, T. von, L. M. Thorpe, S. R. Walker, T. M. Roberts, D. A. Frank, J. J. Zhao, NTRK2 activation cooperates with PTEN deficiency in T-ALL through activation of both the PI3K–AKT and JAK–STAT3 pathways. *Cell Discov.* **2**, 16030 (2016).
36. S. F. Moore, M. T. J. van den Bosch, R. W. Hunter, K. Sakamoto, A. W. Poole, I. Hers, Dual regulation of glycogen synthase kinase 3 (GSK3)α/β by protein kinase C (PKC)α and Akt promotes thrombin-mediated integrin αIIbβ3 activation and granule secretion in platelets. *J. Biol. Chem.* **288**, 3918–3928 (2013).
37. I. Hers, E. E. Vincent, J. M. Tavaré, Akt signalling in health and disease. *Cell. Signal.* **23**, 1515–1527 (2011).
38. D. Papadopoli, M. Pollak, I. Topisirovic, The role of GSK3 in metabolic pathway perturbations in cancer. *Biochim. Biophys. Acta Mol. Cell Res.* **1868**, 119059 (2021).
39. M. M.-K. Wong, S. M. Joyson, H. Hermeking, S. K. Chiu, Transcription factor AP4 mediates cell fate decisions: To divide, age, or die. *Cancers (Basel)* **13**, 676 (2021).
40. J. Wei, P. Yang, T. Zhang, Z. Chen, W. Chen, L. Wanglin, F. He, F. Wei, D. Huang, J. Zhong, Z. Yang, H. Chen, H. Hu, S. Zeng, Z. Sun, J. Cao, Overexpression of transcription factor activating enhancer binding protein 4 (TFAP4) predicts poor prognosis for colorectal cancer patients. *Exp. Ther. Med.* **14**, 3057–3061 (2017).
41. C. Chou, A. K. Pinto, J. D. Curtis, S. P. Persaud, M. Cella, C.-C. Lin, B. T. Edelson, P. M. Allen, M. Colonna, E. L. Pearce, M. S. Diamond, T. Egawa, c-Myc-induced transcription factor AP4 is required for host protection mediated by $CD8^+$ T cells. *Nat. Immunol.* **15**, 884–893 (2014).
42. F. Blaeschke, Y. Y. Chen, R. Apathy, B. Daniel, A. Y. Chen, P. A. Chen, K. Sandor, W. Zhang, Z. Li, C. T. Mowery, T. N. Yamamoto, W. A. Nyberg, A. To, R. Yu, R. Bueno, M. C. Kim, R. Schmidt, D. B. Goodman, T. Feuchtinger, J. Eyquem, C. Jimmie Ye, J. Carnevale, A. T. Satpathy, E. Shifrut, T. L. Roth, A. Marson, Modular pooled discovery of synthetic knockin sequences to program durable cell therapies. *Cell* **186**, 4216–4234.e33 (2023).
43. J. Yang, J. P. Ma, S. Xiao, X. H. Zhang, J. B. Xu, C. Q. Chen, S. R. Cai, Y. L. He, Evaluating the prognostic value and functional roles of transcription factor AP4 in colorectal cancer. *Oncol. Lett.* **15**, 7545–7554 (2018).
44. C. Chen, Q. Cai, W. He, T. B. Lam, J. Lin, Y. Zhao, X. Chen, P. Gu, H. Huang, M. Xue, H. Liu, F. Su, J. Huang, J. Zheng, T. Lin, AP4 modulated by the PI3K/AKT pathway promotes prostate cancer proliferation and metastasis of prostate cancer via upregulating L-plastin. *Cell Death Dis.* **8**, e3060 (2017).
45. X. Liu, B. Zhang, Y. Guo, Q. Liang, C. Wu, L. Wu, K. Tao, G. Wang, J. Chen, Down-regulation of AP-4 inhibits proliferation, induces cell cycle arrest and promotes apoptosis in human gastric cancer cells. *PLOS ONE* **7**, e37096 (2012).
46. J.-N. Liu, X.-S. Kong, P. Sun, R. Wang, W. Li, Q.-F. Chen, An integrated pan-cancer analysis of TFAP4 aberrations and the potential clinical implications for cancer immunity. *J. Cell. Mol. Med.* **25**, 2082–2097 (2021).
47. C. Luo, J. Shen, Adducin in tumorigenesis and metastasis. *Oncotarget* **8**, 48453–48459 (2017).
48. S. Kandel, P. Adhikary, G. Li, K. Cheng, The TIM3/Gal9 signaling pathway: An emerging target for cancer immunotherapy. *Cancer Lett.* **510**, 67–78 (2021).
49. D. Compagno, C. Tiraboschi, J. D. Garcia, Y. Rondón, E. Corapi, C. Velazquez, D. J. Laderach, Galectins as checkpoints of the immune system in cancers, their clinical relevance, and implication in clinical trials. *Biomolecules* **10**, 750 (2020).
50. J. Joung, S. Konermann, J. S. Gootenberg, O. O. Abudayyeh, R. J. Platt, M. D. Brigham, N. E. Sanjana, F. Zhang, Genome-scale CRISPR-Cas9 knockout and transcriptional activation screening. *Nat. Protoc.* **12**, 828–863 (2017).
51. P. A. Ewels, A. Peltzer, S. Fillinger, H. Patel, J. Alneberg, A. Wilm, M. U. Garcia, P. Di Tommaso, S. Nahnsen, The nf-core framework for community-curated bioinformatics pipelines. *Nat. Biotechnol.* **38**, 276–278 (2020).
52. Y. Zhang, T. Liu, C. A. Meyer, J. Eeckhoute, D. S. Johnson, B. E. Bernstein, C. Nusbaum, R. M. Myers, M. Brown, W. Li, X. S. Liu, Model-based analysis of ChIP-Seq (MACS). *Genome Biol.* **9**, R137 (2008).
53. J. T. Robinson, H. Thorvaldsdóttir, W. Winckler, M. Guttman, E. S. Lander, G. Getz, J. P. Mesirov, Integrative genomics viewer. *Nat. Biotechnol.* **29**, 24–26 (2011).
54. Y. Liao, G. K. Smyth, W. Shi, featureCounts: An efficient general purpose program for assigning sequence reads to genomic features. *Bioinformatics* **30**, 923–930 (2014).
55. M. D. Robinson, D. J. McCarthy, G. K. Smyth, edgeR: A Bioconductor package for differential expression analysis of digital gene expression data. *Bioinformatics* **26**, 139–140 (2010).
56. M. R. Mumbach, A. T. Satpathy, E. A. Boyle, C. Dai, B. G. Gowen, S. W. Cho, M. L. Nguyen, A. J. Rubin, J. M. Granja, K. R. Kazane, Y. Wei, T. Nguyen, P. G. Greenside, M. R. Corces, J. Tycko, D. R. Simeonov, N. Suliman, R. Li, J. Xu, R. A. Flynn, A. Kundaje, P. A. Khavari, A. Marson, J. E. Corn, T. Quertermous, W. J. Greenleaf, H. Y. Chang, Enhancer connectome in primary human cells identifies target genes of disease-associated DNA elements. *Nat. Genet.* **49**, 1602–1612 (2017).
57. M. R. Mumbach, A. J. Rubin, R. A. Flynn, C. Dai, P. A. Khavari, W. J. Greenleaf, H. Y. Chang, HiChIP: Efficient and sensitive analysis of protein-directed genome architecture. *Nat. Methods* **13**, 919–922 (2016).

58. N. Servant, N. Varoquaux, B. R. Lajoie, E. Viara, C. J. Chen, J. P. Vert, E. Heard, J. Dekker, E. Barillot, HiC-Pro: An optimized and flexible pipeline for Hi-C data processing. *Genome Biol.* **16**, 259 (2015).
59. J. Wolff, L. Rabbani, R. Gilsbach, G. Richard, T. Manke, R. Backofen, B. A. Grüning, Galaxy HiCExplorer 3: A web server for reproducible Hi-C, capture Hi-C and single-cell Hi-C data analysis, quality control and visualization. *Nucleic Acids Res.* **48**, W177–W184 (2020).
60. J. Wolff, V. Bhardwaj, S. Nothjunge, G. Richard, G. Renschler, R. Gilsbach, T. Manke, R. Backofen, F. Ramírez, B. A. Grüning, Galaxy HiCExplorer: A web server for reproducible Hi-C data analysis, quality control and visualization. *Nucleic Acids Res.* **46**, W11–W16 (2018).
61. F. Ramírez, D. P. Ryan, B. Grüning, V. Bhardwaj, F. Kilpert, A. S. Richter, S. Heyne, F. Dündar, T. Manke, deepTools2: A next generation web server for deep-sequencing data analysis. *Nucleic Acids Res.* **44**, W160–W165 (2016).
62. C. Shi, M. Rattray, G. Orozco, HiChIP-Peaks: A HiChIP peak calling algorithm. *Bioinformatics* **36**, 3625–3631 (2020).
63. C. A. Lareau, M. J. Aryee, hichipper: A preprocessing pipeline for calling DNA loops from HiChIP data. *Nat. Methods* **15**, 155–156 (2018).
64. J. Roels, J. van Hulle, M. Lavaert, A. Kuchmiy, S. Strubbe, T. Putteman, B. Vandekerckhove, G. Leclercq, F. van Nieuwerburgh, L. Boehme, T. Taghon, Transcriptional dynamics and epigenetic regulation of E and ID protein encoding genes during human T cell development. *Front. Immunol.* **13**, 960918 (2022).
65. J. Roels, A. Kuchmiy, M. de Decker, S. Strubbe, M. Lavaert, K. L. Liang, G. Leclercq, B. Vandekerckhove, F. van Nieuwerburgh, P. van Vlierberghe, T. Taghon, Distinct and temporary-restricted epigenetic mechanisms regulate human αβ and γδ T cell development. *Nat. Immunol.* **21**, 1280–1292 (2020).
66. G. Monaco, B. Lee, W. Xu, S. Mustafah, Y. Y. Hwang, C. Carré, N. Burdin, L. Visan, M. Ceccarelli, M. Poidinger, A. Zippelius, J. Pedro de Magalhães, A. Larbi, RNA-Seq signatures normalized by mRNA abundance allow absolute deconvolution of human immune cell types. *Cell Rep.* **26**, 1627–1640.e7 (2019).
67. B. Squiban, S. T. Ahmed, J. K. Frazer, Creation of a human T-ALL cell line online database. *Leuk. Lymphoma* **58**, 2728–2730 (2017).

Acknowledgments: We thank the members of the Knoechel and Lohr Lab for helpful discussions and critical comments on the manuscript. We thank the DFCI flow core for assistance with flow sorting. **Funding:** This study was supported by the NIH (R01CA249185 to B.K.), a Damon Runyon Clinical Investigator Award (B.K.), Hyundai Hope on Wheels (B.K.), Cookies for Kid's Cancer (B.K.), the Rally Foundation for Childhood Cancer (B.K.), NIH R01CA193651 (A.G.), NIH R01 CA249678 (A.G.), the V Foundation for Cancer Research (A.G.), and ALSAC (A.G.). **Author contributions:** C.R.M.W.: Writing—original draft, conceptualization, investigation, writing—review and editing, methodology, resources, data curation, validation, supervision, formal analysis, software, project administration, and visualization. B.Y.: Writing—original draft, conceptualization, investigation, writing—review and editing, methodology, resources, data curation, validation, supervision, formal analysis, project administration, and visualization. N.G.T.: Investigation, methodology, validation, supervision, project administration, and visualization. T.B.H.-F.: Investigation and supervision. E.Y.C.: Investigation and formal analysis. Z.C.E.: Investigation and methodology. M.O.: Investigation. S.B.K.: Investigation. Y.C.-C.: Investigation. A.G.: Conceptualization, writing—review and editing, methodology, supervision, and formal analysis. J.G.L.: Writing—original draft, conceptualization, writing—review and editing, methodology, resources, funding acquisition, data curation, validation, supervision, and project administration. B.K.: Writing—original draft, conceptualization, writing—review and editing, methodology, resources, funding acquisition, validation, supervision, and project administration. **Competing interests:** J.G.L. received research funding from Bristol Myers Squibb for an unrelated project. A.G. is a consultant and advisory board member of Attivare Therapeutics. The other authors declare that they have no competing interests. **Data and materials availability:** All data needed to evaluate the conclusions in the paper are present in the paper and/or the Supplementary Materials. The data generated in this study are publicly available in NCBI Gene Expression Omnibus at GSE275039 (ChIP-seq), GSE275040 (HiChIP-seq), and GSE275043 (CRISPR screen).

Submitted 4 September 2024
Accepted 12 February 2025
Published 19 March 2025
10.1126/sciadv.ads8351